BIOCHEMISTRY
including biophysical chemistry & molecular biology
Article

Biochemistry **2010,** *49,* 6655–6669 6655
DOI: 10.1021/bi100730d

Evidence from FTIR Difference Spectroscopy of an Extensive Network of Hydrogen Bonds near the Oxygen-Evolving Mn_4Ca Cluster of Photosystem II Involving D1-Glu65, D2-Glu312, and D1-Glu329[†]

Rachel J. Service,[‡] Warwick Hillier,[§] and Richard J. Debus*,[‡]

[‡]*Department of Biochemistry, University of California, Riverside, California 92521, and* [§]*Photobioenergetics Group, Research School of Biological Sciences, The Australian National University, Canberra, ACT, Australia 0200*

Received May 9, 2010; Revised Manuscript Received July 1, 2010

ABSTRACT: Analyses of the refined X-ray crystallographic structures of photosystem II (PSII) at 2.9−3.5 Å have revealed the presence of possible channels for the removal of protons from the catalytic Mn_4Ca cluster during the water-splitting reaction. As an initial attempt to verify these channels experimentally, the presence of a network of hydrogen bonds near the Mn_4Ca cluster was probed with FTIR difference spectroscopy in a spectral region sensitive to the protonation states of carboxylate residues and, in particular, with a negative band at 1747 cm^{-1} that is often observed in the S_2-minus-S_1 FTIR difference spectrum of PSII from the cyanobacterium *Synechocystis* sp. PCC 6803. On the basis of its 4 cm^{-1} downshift in D_2O, this band was assigned to the carbonyl stretching vibration (C=O) of a protonated carboxylate group whose pK_a decreases during the S_1 to S_2 transition. The positive charge that forms on the Mn_4Ca cluster during the S_1 to S_2 transition presumably causes structural perturbations that are transmitted to this carboxylate group via electrostatic interactions and/or an extended network of hydrogen bonds. In an attempt to identify the carboxylate group that gives rise to this band, the FTIR difference spectra of PSII core complexes from the mutants D1-Asp61Ala, D1-Glu65Ala, D1-Glu329Gln, and D2-Glu312Ala were examined. In the X-ray crystallographic models, these are the closest carboxylate residues to the Mn_4Ca cluster that do not ligate Mn or Ca and all are highly conserved. The 1747 cm^{-1} band is present in the S_2-minus-S_1 FTIR difference spectrum of D1-Asp61Ala but absent from the corresponding spectra of D1-Glu65Ala, D2-Glu312Ala, and D1-Glu329Gln. The band is also sharply diminished in magnitude in the wild type when samples are maintained at a relative humidity of ≤85%. It is proposed that D1-Glu65, D2-Glu312, and D1-Glu329 participate in a common network of hydrogen bonds that includes water molecules and the carboxylate group that gives rise to the 1747 cm^{-1} band. It is further proposed that the mutation of any of these three residues, or partial dehydration caused by maintaining samples at a relative humidity of ≤85%, disrupts the network sufficiently that the structural perturbations associated with the S_1 to S_2 transition are no longer transmitted to the carboxylate group that gives rise to the 1747 cm^{-1} band. Because D1-Glu329 is located approximately 20 Å from D1-Glu65 and D2-Glu312, the postulated network of hydrogen bonds must extend for at least 20 Å across the lumenal face of the Mn_4Ca cluster. The D1-Asp61Ala, D1-Glu65Ala, and D2-Glu312Ala mutations also appear to substantially decrease the fraction of PSII reaction centers that undergo the S_3 to S_0 transition in response to a saturating flash. This behavior is consistent with D1-Asp61, D1-Glu65, and D2-Glu312 participating in a dominant proton egress channel that links the Mn_4Ca cluster with the thylakoid lumen.

The light-driven oxidation of water in photosystem II (PSII)[1] produces nearly all of the O_2 on Earth and drives the production of nearly all of its biomass. Photosystem II is an integral membrane protein complex that is located in the thylakoid membranes of plants, algae, and cyanobacteria. It is a homodimer in vivo, having a total molecular mass of > 700 kDa. Each monomer consists of at least 20 different subunits and contains more than 60 organic and inorganic cofactors, including 35 Chl *a* and 12 carotenoid molecules. Each monomer's primary subunits include the membrane spanning polypeptides CP47 (56 kDa), CP43 (52 kDa), D2 (39 kDa), and D1 (38 kDa) and the extrinsic polypeptide PsbO (26.8 kDa). The D1 and D2 polypeptides are homologous and together form a heterodimer at the core of each monomer. Within each monomer, the CP47 and CP43 polypeptides are located on either side of the D1−D2 heterodimer and serve to transfer excitation energy from the peripherally located antenna complex to the D1−D2 heterodimer, and specifically to the photochemically active Chl *a* multimer known as P_{680} (*1*−*6*).

[†]Support for this work was provided by the National Institutes of Health (Grant GM 076232 to R.J.D.) and by the Australian Research Council (Grant FT0990972 to W.H.).

*To whom correspondence should be addressed. Phone: (951) 827-3483. Fax: (951) 827-4434. E-mail: richard.debus@ucr.edu.

[1]Abbreviations: Chl, chlorophyll; EDTA, ethylenediaminetetraacetic acid; EPR, electron paramagnetic resonance; EXAFS, extended X-ray absorption fine structure; FTIR, Fourier transform infrared; MES, 2-(*N*-morpholino)ethanesulfonic acid; NTA, nitrilotriacetic acid; P_{680}, chlorophyll multimer that serves as the light-induced electron donor in PSII; Pheo, pheophytin; PSII, photosystem II; Q_A, primary plastoquinone electron acceptor; Q_B, secondary plastoquinone electron acceptor; RH, relative humidity; XANES, X-ray absorption near edge structure; Y_Z, tyrosine residue that mediates electron transfer between the Mn_4Ca cluster and $P_{680}^{+\bullet}$; Y_D, second tyrosine residue that can reduce $P_{680}^{+\bullet}$ in PSII.

Published on Web 07/01/2010

The O_2-evolving catalytic site consists of a pentanuclear metal cluster containing four Mn ions and one Ca ion. The Mn_4Ca cluster accumulates oxidizing equivalents in response to photochemical events within PSII and then catalyzes the oxidation of two molecules of water, releasing one molecule of O_2 as a byproduct (*7*−*11*). The Mn_4Ca cluster serves as the interface between single-electron photochemistry and the four-electron process of water oxidation. The photochemical events that precede water oxidation take place in the D1−D2 heterodimer. These events are initiated by the transfer of excitation energy to P_{680} following capture of light energy by the antenna complex. Excitation of P_{680} results in the formation of the charge-separated state, $P_{680}^{\bullet+}Pheo^{\bullet-}$. This light-induced separation of charge is stabilized by the rapid oxidation of $Pheo^{\bullet-}$ by Q_A, the primary plastoquinone electron acceptor, and by the rapid reduction of $P_{680}^{\bullet+}$ by Y_Z, one of two redox-active tyrosine residues in PSII. The resulting $Y_Z^{\bullet}$ radical in turn oxidizes the Mn_4Ca cluster, while $Q_A^{\bullet-}$ reduces the secondary plastoquinone, Q_B. Subsequent charge separations result in further oxidation of the Mn_4Ca cluster and in the two-electron reduction and protonation of Q_B to form plastoquinol, which subsequently exchanges into the membrane-bound plastoquinone pool. During each catalytic cycle, two molecules of plastoquinol are produced at the Q_B site and the Mn_4Ca cluster cycles through five oxidation states termed S_n, where n denotes the number of oxidizing equivalents that are stored (n = 0−4). The S_1 state predominates in dark-adapted samples. Most interpretations of Mn-XANES data have concluded that the S_1 state consists of two Mn(III) and two Mn(IV) ions and that the S_2 state consists of one Mn(III) and three Mn(IV) ions (*11*−*14*). The S_4 state is a transient intermediate. Its formation triggers the rapid oxidation of the two substrate water molecules, the regeneration of the S_0 state, and the release of O_2.

Refined X-ray crystallographic structural models of PSII are available at 3.5 (*1*), 3.0 (*2*), and 2.9 Å (*5*) (although the 2.9 Å structural model was developed by reprocessing the data used for the 3.0 Å model). These models, and less complete models at somewhat lower resolutions (*15*, *16*), provide views of the Mn_4Ca cluster and its ligation environment, including one or two catalytically essential Cl^- ions that are located 6−7 Å distant. However, there are significant differences between these views. For example, in the 2.9 and 3.0 Å structural models, most carboxylate ligands are bidentate and the α-COO^- group of D1-Ala344 (the C-terminus of the D1 polypeptide) ligates the Mn_4Ca cluster, whereas in the 3.5 Å structural model, most carboxylate ligands are unidentate and the α-COO^- group of D1-Ala344 ligates no metal ion. One reason for these differences is that the resolutions of the diffraction data are limited. A second reason is that the Mn(III/IV) ions of the Mn_4Ca cluster were undoubtedly reduced by X-ray-generated radicals to their fully reduced Mn(II) oxidation states during collection of the X-ray diffraction data (*17*, *18*). This reduction would have disrupted the cluster's Mn−O−Mn bridging moieties and altered Mn−ligand interactions. Consequently, the structures of the Mn_4Ca cluster depicted in the X-ray crystallographic models represent unknown superimpositions of native and disrupted Mn_4Ca clusters, with the metal ions in the latter being retained in the vicinity of their native positions by virtue of the crystals being kept frozen at 100 K during data collection. Importantly, none of the crystallographic structural models is fully compatible with polarized EXAFS studies of single crystals of PSII that were conducted with low X-ray fluxes that minimize photoreduction of the Mn ions (*19*). The low-radiation flux studies must be reconciled with future X-ray crystallographic studies. Nevertheless, the existing crystallographic studies agree with each other, and with the earlier mutagenesis studies (*20*), on the identity of most of the Mn_4Ca cluster's amino acid ligands. Furthermore, the structure of PSII outside the immediate environment of the Mn_4Ca cluster should be largely unaffected by the radiation-induced reduction of the cluster's Mn ions. Consequently, the existing crystallographic structural models are serving as valuable guides for spectroscopic studies designed to provide insight into the structure, dynamics, and mechanism of the Mn_4Ca cluster throughout its catalytic cycle.

To satisfy the very severe energetic and mechanistic constraints of oxidizing water, the Mn_4Ca cluster's reactivity in each of its oxidation states is tightly controlled by its protein environment. The amino acid residues in this environment choreograph the proton and electron reactions associated with water oxidation and play important roles in the delivery of substrate water and the release of O_2 and protons. In particular, these residues minimize the energetic requirements for water oxidation by coupling the requisite proton and electron extraction reactions (*7*, *13*, *21*, *22*), minimize deleterious side reactions by preventing unregulated access of water to the Mn_4Ca catalyst (*23*), and minimize oxidative damage by promoting rapid egress of newly formed O_2 (*24*). For example, the deprotonation of CP43-Arg357 or D1-Asp61 to the thylakoid lumen has been proposed to provide the thermodynamic driving force for oxidizing the Mn_4Ca cluster in its higher oxidation states (*7*, *13*, *21*, *22*, *25*−*28*). Deprotonation is envisioned to take place via one or more proton egress pathways or "channels". Several possible channels for water access, O_2 egress, and proton egress have been identified in the current crystallographic structural models on the basis of visual examinations (*1*, *29*−*31*), electrostatic calculations (*32*), solvent accessibility simulations (*33*), cavity searching algorithms (*5*, *34*, *35*), and molecular dynamics simulations of water diffusion (*36*). In the 2.9 Å structural model, nine discrete channels have been identified on the basis of cavity searching algorithms, including four attributed to water access or O_2 egress channels and five attributed to proton egress channels (*5*, *35*). These predicted channels are presumably dynamic in nature and presumably contain extensive networks of hydrogen-bonded amino acid side chains and water molecules. Our goal is to employ FTIR difference spectroscopy to further delineate the proton egress pathways leading from the Mn_4Ca cluster to the lumen and to determine if multiple pathways are active or if a single pathway dominates. Such a situation prevails in reaction centers of *Rhodobacter sphaeroides*, where a single proton entry point and a single proton access channel dominate the transfer of protons to the Q_B site (*37*−*39*).

FTIR difference spectroscopy is an extremely sensitive tool for characterizing the dynamic structural changes that occur during an enzyme's catalytic cycle (*40*−*44*). It is particularly suited for analyzing protonation−deprotonation reactions, pK_a shifts, and changes in hydrogen-bonded structures in proteins. The carbonyl stretching mode [ν(C=O)] of a protonated carboxylate residue appears between 1770 and 1700 cm^{-1}, a region where no other protein bands occur. The actual frequency of this mode depends on the number and strengths of hydrogen bonds involving this group (*45*−*49*). The O−H stretching frequency of weakly hydrogen bonded O−H groups appears between 3700 and 3500 cm^{-1} (*50*−*52*), the O−D stretching frequency of weakly deuteron-bonded O−D groups between 2600 and 2200 cm^{-1} (*51*), and the D−O−D bending region of D_2O molecules

between 1250 and 1150 cm^{-1} (*53*, *54*), also in a region mostly devoid of other protein vibrational modes. This mode is also sensitive to hydrogen (deuteron) bonding and disappears upon deprotonation, making it particularly suitable for monitoring proton release reactions. Changes in the hydrogen bonding status of amino acid residues and water molecules participating in putative water access or proton egress pathways can be monitored at these easily accessible frequencies.

In PSII, numerous vibrational modes are altered in frequency as the Mn_4Ca cluster is oxidized through the S state cycle, including many modes that can be attributed to carboxylate residues and hydrogen-bonded water molecules (*55*−*57*). In this study, on the basis of the presence or absence of the ν(C=O) mode of a protonated carboxylate group in the S_2-minus-S_1 FTIR difference spectrum, we present evidence that residues D1-Glu65, D1-Glu329, and D2-Glu312 participate in a hydrogen-bonded network that extends at least 20 Å across the lumenal face of the Mn_4Ca cluster. This network presumably also includes D1-Asp61. The D1-D61A, D1-E65A, and D2-E312A mutations were also found to substantially decrease the fraction of PSII reaction centers that undergo the S_3 to S_0 transition in response to a saturating flash. Consequently, the hydrogen-bonded network that includes D1-Asp61, D1-Glu65, D2-Glu312, and D1-Glu329 may comprise part of a dominant proton egress pathway leading from the Mn_4Ca cluster to the thylakoid lumen. The participation of D1-Asp61, D1-Glu65, and D2-Glu312 in such a pathway has been proposed previously (*1*, *5*, *32*−*35*), but the participation of D1-Glu329 in the same network is unexpected because it is located far from any proposed proton egress channel.

MATERIALS AND METHODS

Construction of Mutants and Propagation of Cultures. The D1-D61A, D1-E65A, and D1-E329Q mutations were constructed in the *psbA-2* gene of *Synechocystis* sp. PCC 6803 (*58*) and transformed into a host strain of *Synechocystis* that lacks all three *psbA* genes and contains a hexahistidine tag (His tag) fused to the C-terminus of CP47 (*59*). Single colonies were selected for their ability to grow on solid media containing 5 μg/mL kanamycin monosulfate. The D2-E312A mutation was constructed in the *psbD-1* gene of *Synechocystis* sp. PCC 6803 (*60*) and transformed into a host strain of *Synechocystis* that lacks both *psbD* genes and contains a hexahistidine tag (His tag) fused to the C-terminus of CP47 (*59*). Single colonies were also selected for their ability to grow on solid media containing 5 μg/mL kanamycin monosulfate. Solid media contained 5 mM glucose and 10 μM DCMU. The DCMU and antibiotic were omitted from the liquid cultures. Large-scale liquid cultures (each consisting of three 7 L cultures held in glass carboys) were propagated as described previously (*61*). To verify the integrity of the mutant cultures that were harvested for the purification of PSII core complexes, an aliquot of each culture was set aside and the sequence of the relevant portions of the *psbA-2* or *psbD-1* gene was obtained after PCR amplification of genomic DNA (*58*).

Purification of PSII Core Complexes. Oxygen-evolving PSII core complexes were purified under dim green light at 4 °C with Ni-NTA superflow affinity resin (Qiagen, Valencia, CA) as described previously (*62*). The purification buffer consisted of 1.2 M betaine, 10% (v/v) glycerol, 50 mM MES-NaOH (pH 6.0), 20 mM $CaCl_2$, 5 mM $MgCl_2$, 50 mM histidine, 1 mM EDTA, and 0.03% (w/v) *n*-dodecyl β-D-maltoside. The purified PSII core complexes were concentrated to ~1.0 mg of Chl/mL by ultrafiltration, frozen in liquid N_2, and stored at −196 °C (vapor phase nitrogen).

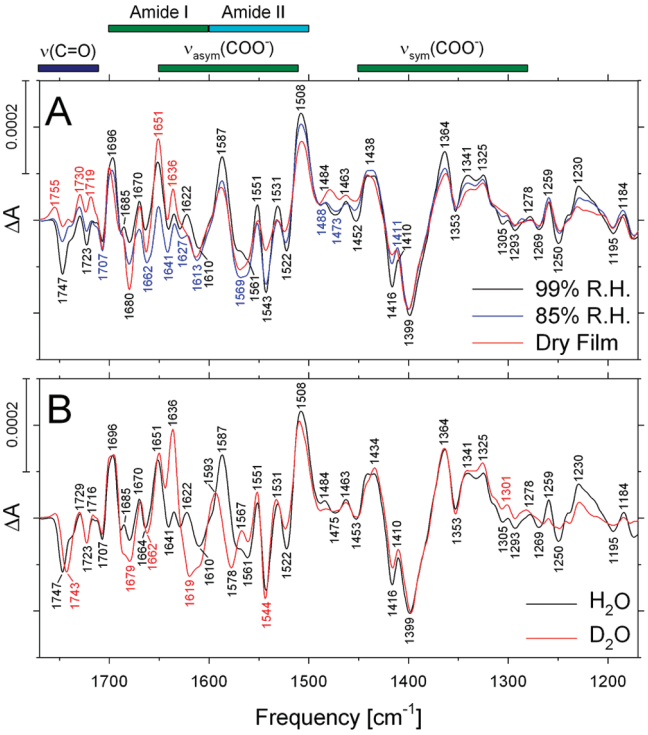

FIGURE 1: Comparison of the midfrequency S_2-minus-S_1 FTIR difference spectra of wild-type PSII core complexes (A) maintained at a relative humidity of 99% (black) or 85% (blue) or as a dry film in the sample cell (red) or (B) exchanged into FTIR buffer containing H_2O (black) or D_2O (red) and maintained at a relative humidity of 99% (in an atmosphere of H_2O or D_2O, respectively). In panel A, the spectra have been normalized to the peak to peak amplitudes of the negative ferricyanide peak at 2115 cm^{-1} and the positive ferrocyanide peak at 2038 cm^{-1}. In panel B, the spectra have been normalized to maximize overlap between 1450 and 1350 cm^{-1}. The black, blue, and red traces in panel A represent the averages of four, seven, and four samples, respectively, and consist of 13800, 24200, and 13400 scans, respectively. The black and red traces in panel B each represent the average of four samples and consist of 13800 and 13600 scans, respectively. The sample temperature was 273 K.

Preparation of FTIR Samples. All manipulations were conducted under dim green light at 4 °C. Samples (approximately 70 μg of Chl *a*) were exchanged into FTIR analysis buffer [40 mM sucrose, 10 mM MES-NaOH (pH 6.0), 5 mM $CaCl_2$, 5 mM NaCl, and 0.06% (w/v) *n*-dodecyl β-D-maltoside (*63*, *64*)] by passage through a centrifugal gel filtration column at 27*g* (*65*). Concentrated samples (approximately 10 μL in volume) were mixed with $^1/_{10}$ volume of fresh 100 mM potassium ferricyanide (dissolved in water), spread to a diameter of ~10 mm on a 15 mm diameter BaF_2 window, and then dried lightly (until tacky) under a stream of dry nitrogen gas. To maintain the humidity of the sample in the FTIR cryostat, 1 μL of a solution of glycerol in water was spotted onto the window, adjacent to the sample, but not touching it (*66*). For most experiments, 1 μL of 20% (v/v) glycerol was employed to maintain the samples at 99% RH. For the experiments depicted in Figure 1A, lower relative humidities were obtained with an increase in the concentration of glycerol in the 1 μL droplet [e.g., 40, 50, and 60% (v/v) glycerol for 95, 85, and 73% RH, respectively (*66*)]. A second IR window with a Teflon spacer (0.5 mm thick) was placed over the first and sealed in place with silicon-free high-vacuum grease. The sample was immediately loaded into the FTIR cryostat and allowed to

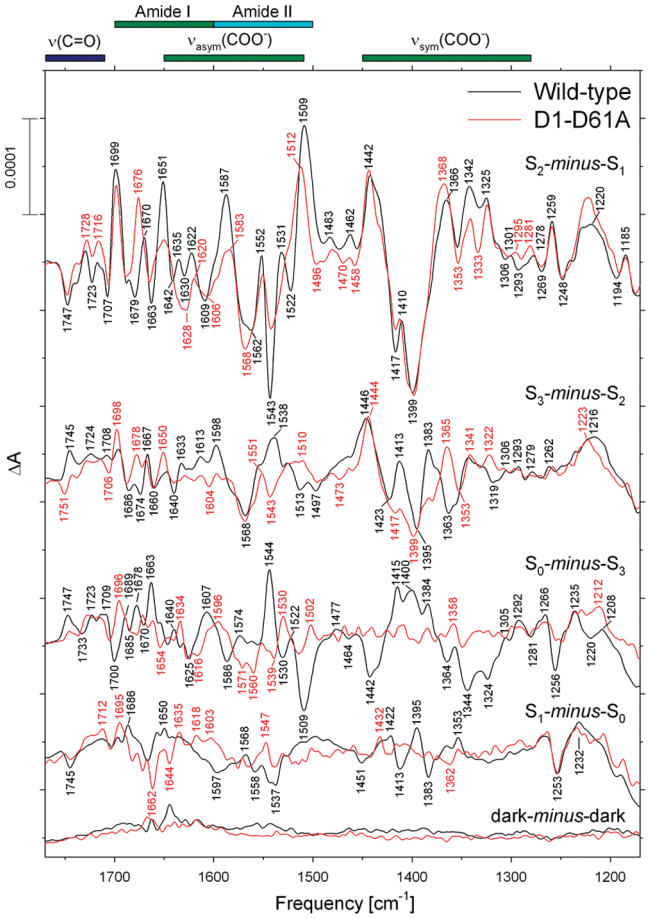

FIGURE 2: Comparison of the midfrequency FTIR difference spectra of wild-type (black) and D1-D61A (red) PSII core complexes in response to four successive flash illuminations applied at 273 K. The wild-type spectra correspond predominantly to the S_2-minus-S_1, S_3-minus-S_2, S_0-minus-S_3, and S_1-minus-S_0 FTIR difference spectra, respectively. The data (plotted from 1770 to 1170 cm^{-1}) represent the averages of nine wild-type and eight D61A samples (10800 and 9600 scans, respectively). To facilitate comparisons, the mutant spectra have been multiplied by factors of ~1.1 after normalization to the peak to peak amplitudes of the negative ferricyanide peak at 2115 cm^{-1} and the positive ferrocyanide peak at 2038 cm^{-1} to maximize overlap with the wild-type spectra. Dark-minus-dark control traces are included to show the noise level (bottom traces).

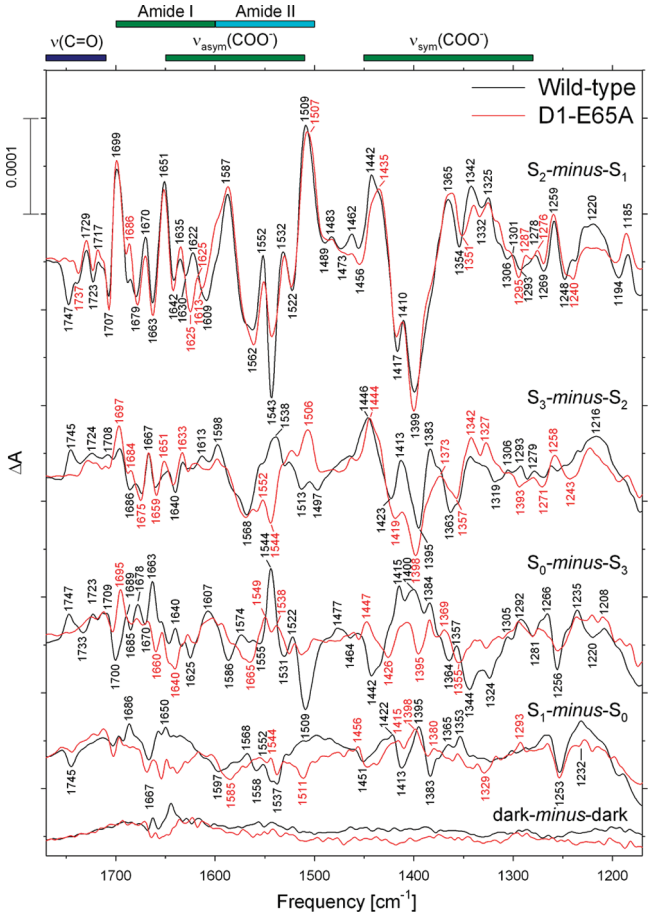

FIGURE 3: Comparison of the midfrequency FTIR difference spectra of wild-type (black) and D1-E65A (red) PSII core complexes in response to four successive flash illuminations applied at 273 K. The data (plotted from 1770 to 1170 cm^{-1}) represent the averages of nine wild-type and 12 D1-D61A samples (10800 and 14400 scans, respectively). To facilitate comparisons, the mutant spectra have been multiplied by factors of ~0.83 after normalization to the peak to peak amplitudes of the negative ferricyanide peak at 2115 cm^{-1} and the positive ferrocyanide peak at 2038 cm^{-1} to maximize overlap with the wild-type spectra. Dark-minus-dark control traces are included to show the noise level (bottom traces).

equilibrate to 273.0 K in darkness for 2 h. Sample concentrations and thicknesses were adjusted so that the absolute absorbance of the amide I band at 1657 cm^{-1} was 0.8−1.2. For the experiments depicted in Figure 1B, the FTIR analysis buffer and the potassium ferricyanide and glycerol solutions were prepared with D_2O (99.9% enrichment, Cambridge Isotope Laboratories, Andover, MA). The pD of the FTIR analysis buffer prepared in D_2O was adjusted with freshly opened NaOD (99.5% enrichment, Cambridge Isotope Laboratories). The pD value was obtained by addition of 0.40 to the pH meter reading (*67*, *68*).

Measurement of FTIR Spectra. Midfrequency FTIR spectra were recorded with a Bruker Equinox 55 spectrometer (Bruker Optics, Billerica, MA) at a spectral resolution of 4 cm^{-1} as described previously (*61*, *64*, *65*). Flash illumination (~20 mJ/flash, ~7 ns fwhm) was provided by a frequency-doubled Q-switched Nd:YAG laser [Surelite I (Continuum, Santa Clara, CA)]. For the experiments depicted in Figure 1, a single flash was applied after dark adaptation. Two single-beam spectra were recorded before the flash, and one single-beam spectrum was recorded starting 0.33 s after the flash (each single-beam spectrum consisted of 200 scans). The 0.33 s delay was incorporated to allow for the oxidation of $Q_A^{\bullet-}$ by the ferricyanide. To obtain a difference spectrum, the spectrum that was recorded after the flash was divided by the spectrum that was recorded immediately before the flash and the ratio was converted to units of absorption. To estimate the background noise level, the second preflash spectrum was divided by the first and the ratio was converted to units of absorption. The sample was dark-adapted for 30 min, and then the measurement cycle was repeated. Each sample was subjected to a total of 16−18 measurement cycles. The difference spectra recorded with several samples were averaged. For the experiments depicted in Figures 2−6, one preflash was applied after dark adaptation and followed by dark adaptation for an additional 5 min. This treatment was employed to oxidize Y_D and to maximize the proportion of PSII reaction centers in the S_1 state. Six successive flashes then were applied with an interval of 12.2 s between each. Two single-beam spectra were recorded before the first flash, and one single-beam spectrum was recorded starting 0.33 s after the first and subsequent flashes (each single-beam spectrum consisted of 100 scans). To obtain difference spectra corresponding to successive

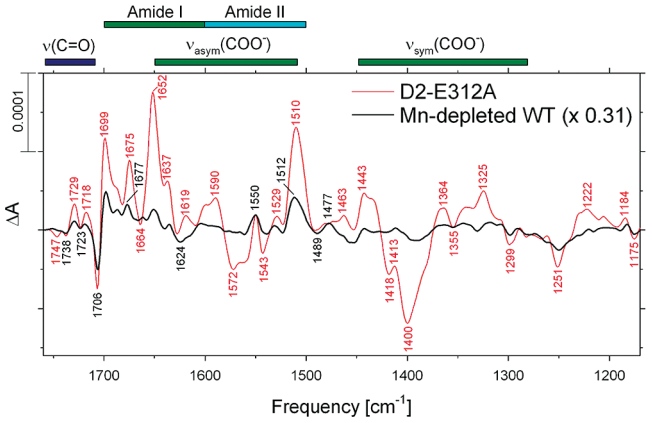

FIGURE 4: Comparison of the midfrequency FTIR difference spectra of Mn-depleted wild-type (black) and intact D2-E312A (red) PSII core complexes in response to the first of six successive flash illuminations applied at 273 K. The data (plotted from 1770 to 1170 cm^{-1}) represent the averages of nine Mn-depleted wild-type and nine D2-E312A samples (10800 scans each). The fraction of D2-E312A PSII reaction centers lacking Mn_4Ca clusters (0.31) was estimated from the amplitude of the negative peak at 1706 cm^{-1} (see the text for details). Accordingly, the spectrum of the Mn-depleted wild-type sample shown in this figure was multiplied by a factor of 0.31 after normalization to the peak to peak amplitudes of the negative ferricyanide peak at 2115 cm^{-1} and the positive ferrocyanide peak at 2038 cm^{-1}.

S state transitions, the spectrum that was recorded after the *n*th flash was divided by the spectrum that was recorded immediately before the *n*th flash and the ratio was converted to units of absorption. To estimate the background noise level, the second preflash spectrum was divided by the first and the ratio was converted to units of absorption. The sample was dark-adapted for 30 min, and then the entire cycle was repeated, including the preflash and the 5 min additional dark adaptation period. The entire cycle was repeated 12 times for each sample, and the difference spectra recorded for several samples were averaged.

Other Procedures. Chlorophyll concentrations and light-saturated, steady state rates of O_2 evolution were measured as described previously (*69*).

RESULTS

Wild-type PSII core complexes from the cyanobacterium *Synechocystis* sp. PCC 6803 frequently exhibit a negative band at 1747 cm^{-1} in the S_2-minus-S_1 FTIR difference spectrum (*61*, *64*, *65*, *70*, *71*) (Figure 1A, black trace). In this study, this band was altered or eliminated by a number of mutations of highly conserved carboxylate residues in the D1 and D2 polypeptides of *Synechocystis* 6803. The 1790−1710 cm^{-1} region contains the C=O carbonyl stretching mode [ν(C=O)] of protonated carboxylate residues (*42*, *43*, *72*) and also the keto and ester C=O vibrations of chlorophyll, pheophytin, heme, and lipids (*73*). In carboxylic acids, the C=O stretching and C−O−H bending modes of the COOH group are weakly coupled. This coupling is removed by deuteration, causing the ν(C=O) mode to downshift by 4−20 cm^{-1} (*45*, *47*−*49*, *72*). Accordingly, to test whether the 1747 cm^{-1} band corresponds to the ν(C=O) mode of a protonated carboxylate residue, the S_2-minus-S_1 FTIR difference spectra of wild-type PSII core complexes was obtained after exchange into buffer containing D_2O (Figure 1B). In D_2O, the 1747 cm^{-1} mode appeared at 1743 cm^{-1}, a downshift of 4 cm^{-1}. Therefore, we attribute it to the ν(C=O) mode of a protonated carboxylate residue whose environment changes during the S_1 to S_2 transition (see Discussion).

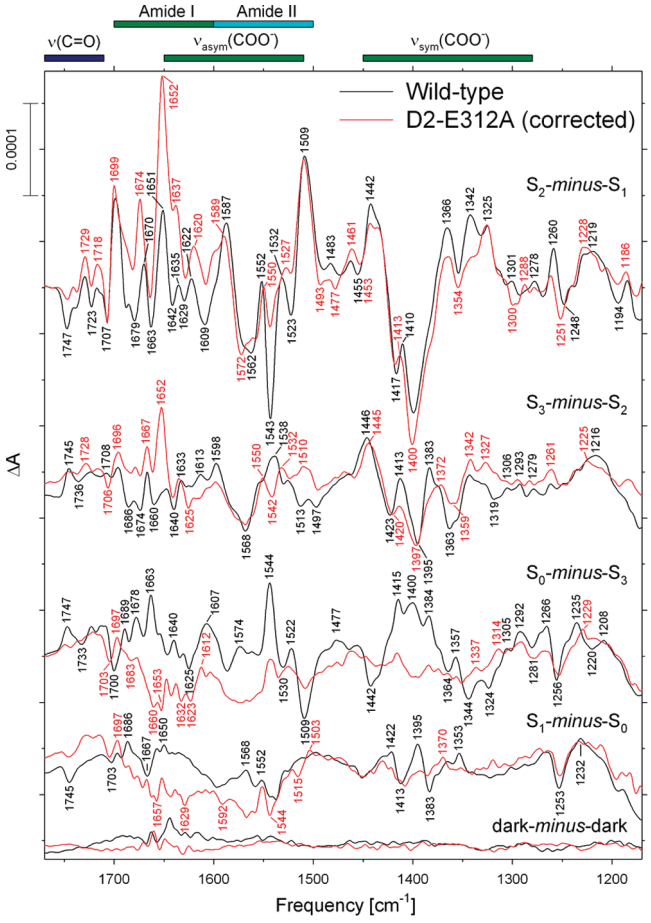

FIGURE 5: Comparison of the midfrequency FTIR difference spectra of wild-type (black) and D2-E312A (red) PSII core complexes in response to four successive flash illuminations applied at 273 K. The data (plotted from 1770 to 1170 cm^{-1}) represent the averages of nine wild-type and nine D2-E312A samples (10800 scans each). The S_2-minus-S_1 FTIR difference spectrum of D2-E312A was corrected for the presence of a significant population of Mn-depleted PSII reaction centers (see the text for details). To facilitate comparisons, the mutant spectra have been multiplied by factors of ~1.4 after normalization to the peak to peak amplitudes of the negative ferricyanide peak at 2115 cm^{-1} and the positive ferrocyanide peak at 2038 cm^{-1} to maximize overlap with the wild-type spectra. Dark-minus-dark control traces are included to show the noise level (bottom traces).

The negative (C=O) band at 1747 cm^{-1} is not observed in PSII core complexes from *Thermosynechococcus elongatus* (*51*, *66*, *74*−*76*) or PSII membranes from spinach (*77*−*80*). Nevertheless, we observe this feature consistently in PSII core complexes from *Synechocystis* sp. PCC 6803 when the samples are maintained at relative humidities of 99% (*61*, *62*, *64*, *65*, *69*) (Figure 1A, black trace) or 95% (not shown). The band has also been observed by others in PSII core complexes purified from the same organism (*70*). In this study, the amplitude of the 1747 cm^{-1} band was diminished substantially at relative humidities of 85% (Figure 1A, blue trace), 73% (not shown), or lower [i.e., when a dry film was placed in the sample cell (Figure 1A, red trace)]. Evidently, the degree of sample hydration is an important factor in the manifestation of this band. Interestingly, whereas other bands in the S_2-minus-S_1 FTIR difference spectrum are sensitive to the degree of sample hydration, none is altered as dramatically at the 1747 cm^{-1} band and many are relatively unperturbed by changes in the sample's relative humidity (see below).

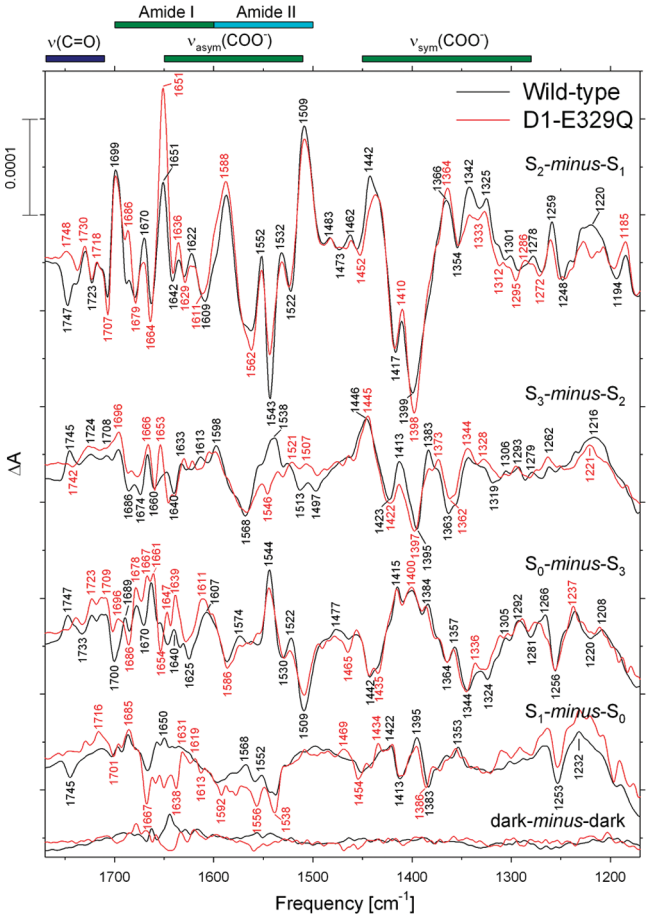

FIGURE 6: Comparison of the midfrequency FTIR difference spectra of wild-type (black) and D1-E329Q (red) PSII core complexes in response to four successive flash illuminations applied at 273 K. The data (plotted from 1770 to 1170 cm^{-1}) represent the averages of nine wild-type and four D1-D329Q samples (10800 and 4800 scans, respectively). The spectra have been normalized to the peak to peak amplitudes of the negative ferricyanide peak at 2115 cm^{-1} and the positive ferrocyanide peak at 2038 cm^{-1}. Dark-minus-dark control traces are included to show the noise level (bottom traces).

Exchange into D_2O induced additional alterations to the wild-type S_2-minus-S_1 FTIR difference spectrum (Figure 1B). The D_2O-induced alterations between 1700 and 1500 cm^{-1} resemble those reported previously in PSII membranes from spinach (*78*) and PSII core complexes from *T. elongatus* (*51*). The apparent upshift of a negative band from 1561 to 1578 cm^{-1} was previously attributed to a D_2O-induced shift of the $\nu_{asym}(COO^-)$ mode of a carboxylate residue that accepts a strong hydrogen bond from a Mn-bound water molecule (*78*). The D_2O-induced alterations to the amide I region, including the appearance of a positive band at 1636 cm^{-1}, were previously attributed to D_2O-induced changes in stretches of polypeptide having random coil conformations (*78*). The apparent upshift of the large positive feature from 1587 to 1593 cm^{-1} is consistent with the D_2O-induced upshift of the $\nu_{asym}(COO^-)$ mode of another hydrogen-bonded carboxylate residue (*78*). The feature has been assigned to a $\nu_{asym}(COO^-)$ mode because it downshifts by 30−35 cm^{-1} after global incorporation of ^{13}C (*63*, *74*, *81*, *82*) but is largely insensitive to global incorporation of ^{15}N (*63*, *74*, *82*).

When the samples were maintained at a relative humidity of ≤85%, spectral alterations were present throughout the overlapping amide II/$\nu_{asym}(COO^-)$ region and in the amide I region, whereas few alterations were present elsewhere (except near 1747 cm^{-1}, as described earlier). Some of the largest alterations were to the 1551(+), 1543(−), 1531(+), and 1522(−) cm^{-1} bands, whose amplitudes decreased substantially. The 1551(+) and 1543(−) cm^{-1} bands were assigned previously to amide II modes because both downshift by 11−20 cm^{-1} after global incorporation of ^{13}C or ^{15}N (*63*, *74*, *78*, *81*, *82*). The 1531(+) and 1522(−) cm^{-1} bands downshift similarly (*63*, *74*, *78*, *81*, *82*) and presumably can also be assigned to amide II modes. The magnitude of a positive band at 1622 cm^{-1} also diminished substantially. This band downshifts significantly after global incorporation of ^{13}C (*63*, *82*), but not appreciably after global incorporation of ^{15}N (*63*, *82*), thereby identifying it as an amide I mode.

The D1-E239Q (*83*) and D2-E312A mutants examined in this study were photoautotrophic, whereas the D1-D61A and D1-E65A cells (*84*) were only weakly so. The O_2 evolving activity of D2-E312A cells was 330−380 μmol of O_2 (mg of Chl)$^{-1}$ h^{-1} compared to 500−580 μmol of O_2 (μg of Chl)$^{-1}$ h^{-1} for wild-type cells (i.e., 60−70% compared to that of the wild type). The O_2 evolving activities of D1-D61A, D1-E65A, and D1-E329Q cells have been reported previously to be ~19, ~21, and ~100% of the wild-type value, respectively (*83*, *84*). The O_2 evolving activities of the D1-D61A, D1-E65A, D1-E329Q, and D2-E312A PSII core particles examined in this study were ~870, ~730, ~3340, and ~1380 μmol of O_2 (mg of Chl)$^{-1}$ h^{-1}, respectively, compared to 4900−5400 μmol of O_2 (mg of Chl)$^{-1}$ h^{-1} for the wild type. The O_2 evolving activity of the D1-D61A PSII core complexes (~17% of that of the wild type) correlated with the lower O_2 evolving activity of D1-D61A cells, but the O_2 evolving activities of the D1-E65A, D1-E329Q, and D2-E312A PSII core complexes (~14, ~65, and ~27%, respectively, of that of the wild type) were lower than in intact cells, suggesting either that the Mn_4Ca clusters in D1-E65A, D1-E329Q, and D2-E312A cells are less stable than those in the wild type or that the S state transitions proceed less efficiently in PSII core complexes purified from these mutants than in intact cells.

The midfrequency FTIR difference spectra of wild-type and D1-D61A PSII core complexes that were induced by four successive flashes are compared in Figure 2 (black and red spectra, respectively). The spectra that were induced by the first, second, third, and fourth flashes given to the wild-type PSII core complexes correspond predominantly to the S_2-minus-S_1, S_3-minus-S_2, S_0-minus-S_3, and S_1-minus-S_0 FTIR difference spectra, respectively. These spectra closely resemble the S_{n+1}-minus-S_n difference spectra that have been reported previously for wild-type PSII core complexes from *Synechocystis* sp. PCC 6803 (*61*, *63*−*65*, *85*). The S_2-minus-S_1 FTIR difference spectrum of D1-D61A PSII core complexes (top red trace in Figure 2) showed substantial differences from the wild-type spectrum throughout the overlapping amide II/$\nu_{asym}(COO^-)$ region. As was the case with partly dehydrated samples (Figure 1A), the magnitudes of the bands at 1552(+), 1543(−), 1531(+), and 1522(−) cm^{-1} were diminished substantially. The magnitudes of positive bands at 1635, 1622, 1587, and 1509 cm^{-1} were also diminished substantially, with the 1587 cm^{-1} band being downshifted to 1583 cm^{-1} and the 1509 cm^{-1} band being upshifted to 1512 cm^{-1}. The 1635 and 1622 cm^{-1} bands can be identified as amide I modes because both downshift significantly after global incorporation of ^{13}C (*63*, *82*), but not appreciably after global incorporation of ^{15}N (*63*, *82*). The 1552(+), 1543(−), 1531(+), and 1522(−) cm^{-1} bands can be identified as amide II modes because all four bands downshift appreciably after global incorporation of ^{13}C (*63*, *74*, *81*, *82*) or ^{15}N (*63*, *74*, *82*). Similarly,

the 1587 cm^{-1} band was previously assigned to a $\nu_{asym}(COO^-)$ mode because it downshifts by 30−35 cm^{-1} after global incorporation of ^{13}C (*63*, *74*, *81*, *82*) but is largely insensitive to the global incorporation of ^{15}N (*63*, *74*, *82*). The 1509 cm^{-1} band appears to consist of overlapping amide II and $\nu_{asym}(COO^-)$ modes (*63*, *74*, *82*). Of particular importance to this study is the fact that the negative band at 1747 cm^{-1} was unaffected by the D1-D61A mutation.

The FTIR difference spectrum induced by the second flash applied to D1-D61A PSII core complexes contained some of the features that are present in the S_2-minus-S_1 FTIR difference spectra of the wild type (compare the top two sets of black and red traces in Figure 2). These include bands at 1543(−), 1510(+), 1399(−), and 1365(+) cm^{-1}. The presence of these bands shows that a significant fraction of D1-D61A PSII reaction centers failed to undergo the S_2 to S_3 transition following the second flash.

The FTIR difference spectra induced by the third and fourth flashes applied to D1-D61A PSII core complexes were practically devoid of features (bottom two red traces in Figure 2). Typically, spectral features that appear during the S_1 to S_2 and S_2 to S_3 transitions in wild-type PSII are reversed during the S_3 to S_0 and S_0 to S_1 transitions (*55*−*57*). If large fractions of PSII reaction centers fail to advance between S states in response to saturating flashes, PSII reaction centers that undergo the S_3 to S_0 or S_0 to S_1 transition after the third or fourth flash, respectively, may have their spectral features canceled by PSII reaction centers undergoing the S_1 to S_2 or S_2 to S_3 transition after these flashes. The absence of clear, distinct peaks after the third and fourth flashes in D1-D61A PSII core complexes shows that a large fraction of D1-D61A PSII core complexes failed to advance beyond the S_3 state in response to the these flashes.

The midfrequency FTIR difference spectra of wild-type and D1-E65A PSII core complexes that were induced by four successive flash illuminations are compared in Figure 3 (black and red spectra, respectively). The S_2-minus-S_1 FTIR difference spectrum of D1-E65A PSII core complexes (top red trace in Figure 3) showed substantial differences from the wild-type spectrum throughout the overlapping amide II/$\nu_{asym}(COO^-)$ region. As was the case with D1-D61A PSII core complexes, the magnitudes of the positive bands at 1622 and 1552 cm^{-1} and the negative band at 1543 cm^{-1} were diminished substantially. As noted above, the 1622 cm^{-1} band corresponds to an amide I mode and the 1552 and 1543 cm^{-1} bands correspond to amide II modes. Of particular importance to this study is the fact that the negative band at 1747 cm^{-1} in the S_2-minus-S_1 FTIR difference spectrum of wild-type PSII core complexes was eliminated by the D1-E65A mutation (compare the top traces in Figure 3).

The FTIR difference spectrum induced by the second flash applied to D1-E65A PSII core complexes contained some of the features present in the S_2-minus-S_1 FTIR difference spectra of the wild type (compare the top two sets of black and red traces in Figure 3). These include bands at 1544(−), 1506(+), 1398(−), and 1373(+) cm^{-1}. The presence of these bands shows that a significant fraction of D1-E65A PSII reaction centers failed to undergo the S_2 to S_3 transition following the second flash. As was observed with D1-D61A, the spectra induced by the third and fourth flashes applied to D1-E65A PSII core complexes are nearly devoid of features (bottom two red traces in Figure 3). Evidently, as was the case with D1-D61A, a large fraction of D1-E65A PSII core complexes fail to advance beyond the S_3 state in response to saturating flashes.

The midfrequency FTIR difference spectrum of D2-E312A PSII core complexes that was induced by the first of six successive flash illuminations is shown in Figure 4 (red spectrum). The presence of a large derivative feature at 1706(−)/1699(+) cm^{-1} suggests that the D2-E312A PSII core complexes contain a significant fraction of PSII reaction centers that lack Mn_4Ca clusters (*61*). The spectrum of Mn-depleted wild-type PSII core complexes obtained under conditions identical to those described in ref *61* is shown for comparison (Figure 4, black trace). This spectrum corresponds to the $Y_Z^{\bullet}$-minus-Y_Z FTIR difference spectrum in *Synechocystis* sp. PCC 6803, whose primary features are positive peaks at 1699, 1677, 1651, 1550, 1521, and 1512 cm^{-1} and negative peaks at 1706, 1624, 1453, and 1250 cm^{-1} (*86*). To estimate the fraction of Mn-depleted PSII reaction centers in the D2-E312A PSII core complexes, the amplitudes of the negative 1706 cm^{-1} band in intact wild-type, Mn-depleted wild-type, and D2-E312A PSII core complexes were compared after normalization of all three spectra to the peak to peak amplitudes of the negative ferricyanide band at 2115 cm^{-1} and the positive ferrocyanide band at 2038 cm^{-1} (i.e., the spectra were normalized to the extent of flash-induced charge separation in each sample, as determined from the reduction of ferricyanide to ferricyanide by $Q_A^{\bullet-}$). On this basis, assuming that 0% of intact and 100% of Mn-depleted wild-type PSII core complexes lack Mn_4Ca clusters, we estimated that ∼31% of D2-E312A PSII core complexes lack Mn_4Ca clusters (presumably the Mn_4Ca clusters in D2-E312A cells are less stable than those in wild-type cells, despite the cluster's distance from D2-Glu312). Accordingly, we corrected the first flash spectrum of the D2-E312A PSII core complexes by subtracting from it 31% of the spectrum of Mn-depleted wild-type PSII (*61*). No correction was applied to the second, third, or fourth flash spectra because Mn-depleted PSII makes no significant contribution to these spectra (*61*).

The midfrequency FTIR difference spectra of wild-type and D2-E312A PSII core complexes that were induced by four successive flash illuminations are compared in Figure 5 (black and red spectra, respectively). The corrected S_2-minus-S_1 FTIR difference spectrum of D1-E312A PSII core complexes (top red trace in Figure 5) showed substantial differences from the wild-type spectrum throughout the overlapping amide II/$\nu_{asym}(COO^-)$ region. As was the case with D1-D61A PSII core complexes, the magnitudes of the bands at 1543(−), 1532(+), and 1523(−) cm^{-1} were diminished substantially. As noted earlier, the 1543(−) and 1532(+) cm^{-1} bands can be identified as amide II modes on the basis of global labeling experiments. Other changes include increased amplitudes of bands at 1674, 1652, and 1637 cm^{-1} in the amide I region, a slight downshift of the positive band at 1622 cm^{-1} [assigned to an amide I mode (see above)], and changes to amplitudes of bands in the symmetric carboxylate stretching region, including decreased amplitudes of positive bands at 1442, 1366, and 1342 cm^{-1} and an increased amplitude of the negative band at 1400 cm^{-1}. Of particular importance to this study is the fact that the negative band at 1747 cm^{-1} in the S_2-minus-S_1 FTIR difference spectrum of wild-type PSII core complexes was eliminated by the D1-E312A mutation (compare the top traces in Figure 5).

The FTIR difference spectrum induced by the second flash applied to D2-E312A PSII core complexes contained some of the features present in the S_2-minus-S_1 FTIR difference spectra of the wild type (compare the top two sets of black and red traces in Figure 5). These include bands at 1542(−), 1510(+), 1397(−), and 1372(+) cm^{-1}. The presence of these bands shows that a

significant fraction of D2-E312A PSII reaction centers failed to undergo the S_2 to S_3 transition following the second flash. As was the case with D1-D61A and D1-E65A, the spectra induced by the third and fourth flashes applied to D1-E312A PSII core complexes were nearly devoid of features (bottom two red traces in Figure 5). Evidently, as was the case with D1-D61A and D1-E65A, a large fraction of D2-E312A PSII core complexes failed to advance beyond the S_3 state in response to these flashes.

The midfrequency FTIR difference spectra of wild-type and D1-E329Q PSII core complexes that were induced by four successive flash illuminations are compared in Figure 6 (black and red spectra, respectively). The S_2-minus-S_1 FTIR difference spectrum of D1-E329Q PSII core complexes (top red trace in Figure 6) showed many fewer differences from the wild-type spectrum than the other mutants. The differences included decreased amplitudes of bands at 1543(−), 1442(+), 1342(+), and 1220(+) cm^{-1} and increased amplitudes of bands at 1651(+), 1635(+), 1398(−), and 1364(+) cm^{-1}. As indicated previously, the 1543(−) and 1635(+) cm^{-1} bands correspond to amide II and amide I modes, respectively. The 1442(+), 1364(+), and 1342(+) cm^{-1} bands correspond to $\nu_{sym}(COO^-)$ modes because they downshift by 20−45 cm^{-1} after global incorporation of ^{13}C (*63*, *74*, *81*, *82*) but are largely insensitive to the global incorporation of ^{15}N (*63*, *74*, *82*).

The FTIR difference spectrum induced by the second flash given to D1-E329Q PSII core complexes contained some of the features present in the S_2-minus-S_1 FTIR difference spectra of wild-type PSII (compare the top two sets of black and red traces in Figure 6). These include bands at 1546(−), 1397(−), and 1373(+) cm^{-1}. The presence of these bands shows that a significant fraction of D1-E329Q PSII reaction centers failed to undergo the S_2 to S_3 transition following the second flash. However, in contrast to the other mutants examined in this study, the FTIR difference spectra induced by the third and fourth flashes resembled those of wild-type PSII core complexes. The primary differences were the slightly diminished amplitudes of the 1544(+) and 1509(−) cm^{-1} bands in the S_0-minus-S_3 FTIR difference spectrum and the minor changes between 1667 and 1538 cm^{-1} in the S_1-minus-S_0 FTIR difference spectrum. Note the similarities between the S_0-minus-S_3 and S_1-minus-S_0 FTIR difference spectra of wild-type and D1-E329Q PSII core complexes between 1450 and 1350 cm^{-1} (compare the bottom two pairs of black and red traces in Figure 6). Evidently, D1-E329Q PSII core complexes advance relatively efficiently between S states in response to saturating laser flashes, in marked contrast to the PSII core complexes of D1-D61A, D1-E65A, and D2-E312A. Of particular importance to this study is the fact that the negative band at 1747 cm^{-1} in the S_2-minus-S_1 FTIR difference spectrum of wild-type PSII core complexes was eliminated by the D1-E329Q mutation (compare the top traces in Figure 6).

It is noteworthy that the second flash spectra of D1-D61A, D1-E65A, D2-E312A, and D1-E329Q PSII core complexes resemble one another (Figures 2, 3, 5, and 6). All four mutant spectra show similar deviations from the wild-type S_3-minus-S_2 FTIR difference spectrum, including negative features at 1546−1542 and 1399−1397 cm^{-1} and positive features at 1510−1506 and 1373−1365 cm^{-1}. The similarities between the second flash spectra of all four mutants suggest that all four mutations decrease the efficiency of the S_2 to S_3 transition to similar extents. In contrast, the essentially featureless third and fourth flash spectra of D1-D61A, D1-E65A, and D2-E312A PSII core complexes show no resemblance to the third or fourth flash spectra of wild-type or D1-E329Q PSII core particles. Evidently, the D1-D61A, D1-E65A, and D2-E312A mutations decrease the efficiency of the S_3 to S_0 transition far more substantially than they decrease the efficiency of the S_2 to S_3 transition.

DISCUSSION

One of the most striking results of the FTIR studies on PSII to date is the stunning insensitivity of the individual FTIR difference spectra to the mutation of at least three of the Mn_4Ca cluster's six putative carboxylate ligands. Not only do mutations of D1-Asp170 (*64*, *87*), D1-Glu189 (*65*, *88*), and D1-Asp342 (*61*) fail to eliminate any carboxylate vibrational stretching modes, they fail to produce significant changes in polypeptide backbone conformations as shown by the lack of significant mutation-induced alterations to the amide I and amide II regions of the spectra. This result was entirely unexpected. The individual FTIR difference spectra of wild-type PSII core complexes contain a wealth of spectral features. It had long been assumed that most of these features would correspond to amino acid residues that ligate the Mn_4Ca cluster. Whereas some of these features clearly correspond to first coordination sphere ligands [i.e., CP43-Glu354 (*71*, *85*) and the α-COO^- group of D1-Ala344 (*62*, *69*, *89*)], the majority of these features evidently correspond to residues in the cluster's second coordination sphere and beyond. These features must reflect the response of the protein to the electrostatic influences that arise from the positive charge that develops on the Mn_4Ca cluster during the S_1 to S_2 transition and to the structural changes that are associated with the S_2 to S_3, S_3 to S_0, and S_0 to S_1 transitions.

The simplest explanation for the insensitivity of the S_2-minus-S_1 FTIR difference spectrum to the individual mutation of most the cluster's putative carboxylate ligands is that the positive charge that develops on the Mn_4Ca cluster during this transition is highly delocalized at ambient temperatures. There is ample precedent for such delocalization in mixed-valence inorganic metal complexes (*90*−*92*). Such delocalization would be consistent with a comparative inelastic X-ray scattering (RIXS) study of Mn oxides, Mn coordination complexes, and spinach PSII membranes (*93*). The authors of this study concluded that the electron that leaves the Mn_4Ca cluster during the S_1 to S_2 transition originates from a highly delocalized orbital (*93*). Delocalization would also be consistent with QM/MM analyses that have been based on the 3.5 Å X-ray crystallographic structural model (*7*, *22*, *27*, *94*). The authors of these studies concluded that the oxidation of the Mn_4Ca cluster during the S_1 to S_2 transition would cause little increase in the electrostatic charge of the individual Mn ions. In their analyses, the greatest increase in electrostatic charge during this transition is actually on the Ca ion. These authors also proposed that the α-COO^- group of D1-Ala344 is a unidentate ligand of Ca. However, a recent ^{13}C ENDOR study shows that this group ligates Mn (*95*) (ligation of both Mn and Ca is possible), consistent with the 3.0 and 2.9 Å crystallographic structural models (*2*, *5*) and with an earlier FTIR study involving the replacement of Ca with Sr (*62*). The QM/MM analyses also predict that CP43-Glu354 ligates along the Jahn−Teller axis of a Mn(III) ion (*7*, *22*, *27*, *94*). On the basis of recent FTIR studies, it has been proposed that CP43-Glu354 changes its coordination mode during the S_1 to S_2 transition (*85*) (but see ref *71*) and that D1-Ala344 significantly changes its orientation (*96*). Consequently, the reason that both the $\nu_{sym}(COO^-)$ mode of D1-Ala344 (*62*, *69*, *89*) and the $\nu_{asym}(COO^-)$ mode of CP43-Glu354 (*71*, *85*) shift during the S_1 to S_2 transition may be that the carboxylate group of one ligates along

the Jahn−Teller axis of the Mn(III) ion that undergoes oxidation and the carboxylate group of the other changes its coordination mode or orientation.

Most of the Mn_4Ca cluster's putative carboxylate ligands appear to facilitate the cluster's assembly (*97*, *98*) rather than regulate its function: D1-Asp170, D1-Glu189, and D1-Asp342 each can be replaced by at least one other amino acid that supports significant O_2 producing activity (*20*, *99*−*101*). In contrast, residues in the Mn_4Ca cluster's second coordination sphere and beyond are postulated to play key roles in providing the driving force for oxidizing the cluster in its higher oxidation states and in regulating the access of substrate water. In particular, recent models postulate that CP43-Arg357 (or D1-Asp61) serves as a redox-activated catalytic base that facilitates the oxidation of the Mn_4Ca cluster during the S_2 to S_3 and S_3 to S_4 transitions (*7*, *13*, *21*, *22*, *25*−*28*). In these models, when the Mn_4Ca cluster is in its S_2 or S_3 state, the formation of $Y_Z^\bullet$ triggers the deprotonation of CP43-Arg357 (or D1-Asp61) to the thylakoid lumen. Protonation to the lumen is necessary from energetic considerations (*102*). The subsequent oxidation of the Mn_4Ca cluster involves the simultaneous transfer of a proton from the Mn_4Ca cluster to the now deprotonated CP43-Arg357 (or D1-Asp61). In these models, the pK_a of CP43-Arg357 (or D1-Asp61) is decreased substantially by the presence of the positive charge on the $Y_Z^\bullet$/D1-His190 pair (hence, the formation of $Y_Z^\bullet$ triggers the residue's deprotonation). The pK_a value is restored when the charge on the $Y_Z^\bullet$/D1-His190 pair is neutralized by the transfer of an electron from the Mn_4Ca cluster to $Y_Z^\bullet$. Hence, the reprotonation of CP43-Arg357 (or D1-Asp61) is highly favored and provides a strong thermodynamic driving force for oxidizing the Mn_4Ca cluster in its higher oxidation states. The initial, $Y_Z^\bullet$-induced deprotonation of CP43-Arg357 (or D1-Asp61) requires its deprotonation to the lumen via a network of protonatable amino acid side chains and water molecules such as those envisaged to exist in the potential proton egress channels that have been identified in the X-ray crystallographic structural models (*1*, *5*, *32*−*35*). Kinetically efficient proton transfer through these channels requires finely tuned pK_a differences between key residues and transient formation of clusters of water molecules (*102*−*105*). Consequently, mutation of key residues in a dominant proton egress pathway would be expected to slow oxidation of the Mn_4Ca cluster in the same manner that mutations that impair proton uptake slow the transfer of an electron from $Q_A^{\bullet-}$ to $Q_B^{\bullet-}$ in reaction centers of *Rhodobacter sphaeroides* (*37*−*39*) and the reduction of O_2 to H_2O in cytochrome *c* oxidase (*106*−*108*). In support of their proposed roles in proton transfer, mutations of D1-Asp61 (*109*−*111*) and CP43-Arg357 (*112*, *113*) slow oxidation of the Mn_4Ca cluster substantially during one or more of the S state transitions.

As an initial attempt to verify the proposed proton egress channels in PSII experimentally, we have used the negative band at 1747 cm^{-1} in the wild-type S_2-minus-S_1 FTIR difference spectrum to probe for the presence of a network of hydrogen bonds near the Mn_4Ca cluster. Residues D1-Asp61, D1-Glu65, D2-Glu312, and D1-Glu329 are highly conserved and are the closest carboxylate residues to the Mn_4Ca cluster that do not ligate Mn or Ca (*1*, *2*, *5*). In the 2.9 Å crystallographic structural model, these residues are located 4.6, 10.8, 11.3, and 7.5 Å from the nearest Mn ion, respectively (*5*) (Figure 7). The peptide carbonyl of D1-Glu329 accepts a hydrogen bond from D1-His332, a putative Mn ligand. The side chain of D1-Glu329 has been proposed to participate in an O_2 egress channel (*5*, *35*),

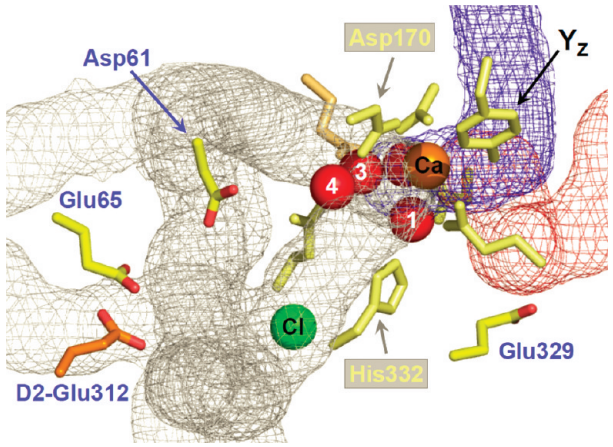

FIGURE 7: Mn_4Ca cluster and its environment as depicted in the 2.9 Å crystallographic structural model of PSII from *T. elongatus* (PDB entry 3BZ1) (*5*). The four residues discussed in this panel are colored bright yellow (Asp61, Glu65, and Glu329 of the D1 polypeptide) or bright orange (Glu312 of the D2 polypeptide). The Mn, Ca, and Cl ions are depicted as red, orange, and green spheres, respectively. Tyrosine Y_Z and the protein ligands of the Mn_4Ca cluster are colored light yellow or orange (residues of D1 and CP43, respectively). Portions of water access, proton egress, and O_2 egress channels identified in the 2.9 Å structural model are colored blue, gray, and maroon, respectively (the channel coordinates from ref *35* were graciously provided by A. Zouni). In this model, the shortest distances between the carboxylate group and the nearest Mn ion are 4.6, 10.8, 11.3, and 7.5 Å for D1-Asp61, D1-Glu65, D2-Glu312, and D1-Glu329, respectively (*5*).

while the side chains of D1-Asp61, D1-Glu65, and D2-Glu312 have been proposed to participate in a proton egress channel (*1*, *5*, *32*−*35*) with D1-Glu65 located at the channel's narrowest point (*5*, *35*).

Our data show that the D1-D61A, D1-E65A, and D2-E312A mutations perturb the properties of the Mn_4Ca cluster far more than do mutations of the putative Mn ligands D1-Asp170, D1-Glu189, and D1-Asp342. The fraction of PSII reaction centers that advance through the S state cycle in response to saturating flashes is substantially diminished in PSII core complexes from all three mutants (Figures 2, 3, and 5). In all three mutants, the efficiency of the S_2 to S_3 transition is lower than in the wild type and the efficiency of the S_3 to S_0 transition appears to be substantially lower. The latter point is best illustrated via comparison of the second and third flash spectra of D1-E329Q with the corresponding data of D1-D61A, D1-E65A, and D2-E312A. Whereas the efficiency of the S_2 to S_3 transition appears to be decreased to similar extents in all four mutants, the efficiency of the S_3 to S_0 transition is much lower in D1-D61A, D1-E65A, and D2-E312A than in D1-E329Q. In contrast, D1-D170H, D1-E189Q, D1-E189R, and D1-D342N PSII core complexes advance efficiently through the S state cycle, with no apparent decrease in the efficiency of any S state transition (*61*, *64*, *65*). A substantially decreased efficiency for the S_3 to S_0 transition in D1-D61A PSII core complexes would be consistent with earlier data showing that the rate of O_2 release is slowed 8-fold in D1-D61A cells (*109*). The D1-D61N mutation also decreases the efficiency of the S state transitions and slows the rate of O_2 release 10-fold (*109*). In D1-D61N PSII core complexes, the S_1 to S_2 and S_2 to S_3 transitions are slowed 2-fold (*109*) and the S_3 to S_0 transition is slowed 10-fold (*110*). A similar slowing of the S state transitions is likely to occur in D1-D61A PSII core complexes and, by inference, in D1-E65A and

D2-E312A PSII core complexes. Slowed oxidation of the Mn_4Ca cluster during the S state transitions would be consistent with a role for all three residues in a dominant postulated proton egress pathway linking the Mn_4Ca cluster with the thylakoid lumen, such as those identified in analyses of the existing X-ray crystallographic structural models (*1*, *5*, *32*−*35*).

The S_2-minus-S_1 FTIR difference spectra of D1-D61A, D1-E65A, D2-E312A, and D1-E329Q PSII core complexes are altered far more than the corresponding spectra of D1-D170H, D1-E189Q, and D1-D342N PSII core complexes. Several amide II modes are altered substantially in the S_2-minus-S_1 FTIR difference spectra of D1-D61A, D1-E65A, and D2-E312A. These alterations show that these mutations alter the conformational rearrangements of the polypeptide backbone that normally accompany the S_1 to S_2 transition. Evidently, the D1-D61A, D1-E65A, and D2-E312A mutations substantially alter part of the protein's structural response to the increased charge that develops on the Mn_4Ca cluster during this transition. The D1-E329Q mutation evidently alters this response to a much lesser extent because only the negative amide II mode at 1543 cm^{-1} is affected significantly.

The primary focus of this study is on the negative band at 1747 cm^{-1}. This band is observed in the S_2-minus-S_1 FTIR difference spectrum of moderately hydrated wild-type PSII core complexes (Figure 8). This band is eliminated by partial dehydration (Figure 8A). It is also eliminated by the D1-E65A, D2-E312A, and D1-E329Q mutations (Figure 8D−F). In contrast, it is unaltered by the D1-D61A mutation (Figure 8C). The elimination of this mode does not correlate with substantial changes in the protein's structural response to the S_1 to S_2 transition because it is present in D1-D61A and absent in D1-E329Q. In carboxylic acids, deuteration removes the weak coupling that exists between the C=O stretching and C−O−H bending modes of the COOH group, causing the ν(C=O) mode to downshift by 4−20 cm^{-1} (*45*, *47*−*49*, *72*). This D_2O-induced downshift is diagnostic for the ν(C=O) mode of protonated carboxylate residues and has been used as such in many systems, including bacteriorhodopsin (*45*, *114*−*117*), rhodopsin (*118*, *119*), bacterial reaction centers (*120*−*123*), heme-copper oxidases (*124*−*127*), and photoactive yellow protein (*128*). Exchange of wild-type PSII core complexes into buffer containing D_2O downshifted the 1747 cm^{-1} band by 4 cm^{-1} (Figure 8B). Deuteration-induced downshifts of 4 cm^{-1} have been reported previously for the ν(C=O) mode of Asp212 in bacteriorhodopsin (*117*), Glu L212 in bacterial reaction centers (*121*), and Glu278 in cytochrome *c* oxidase from *Paracoccus denitrificans* (*124*, *126*) (also see ref *125*). On the basis of its downshift in D_2O, we attribute the negative 1747 cm^{-1} band to the ν(C=O) mode of a protonated carboxylate residue whose environment changes during the S_1 to S_2 transition.

The frequency of the ν(C=O) mode of a carboxylic acid residue depends on the numbers and strengths of hydrogen bonds involving the C=O and O−H groups (*45*, *47*−*49*, *72*). Its appearance at 1747 cm^{-1} in wild-type PSII core complexes suggests that it participates in a single hydrogen bond that involves the C=O group (*48*, *49*), although participation in two hydrogen bonds, with one involving the C−O−H oxygen, cannot be excluded (*49*). In an FTIR difference spectrum, the peak corresponding to the ν(C=O) mode of a carboxylic acid residue can change in a number of ways. Partial protonation (deprotonation) of an Asp or Glu residue gives rise to a single positive (negative) absorption band. Proton transfer between two

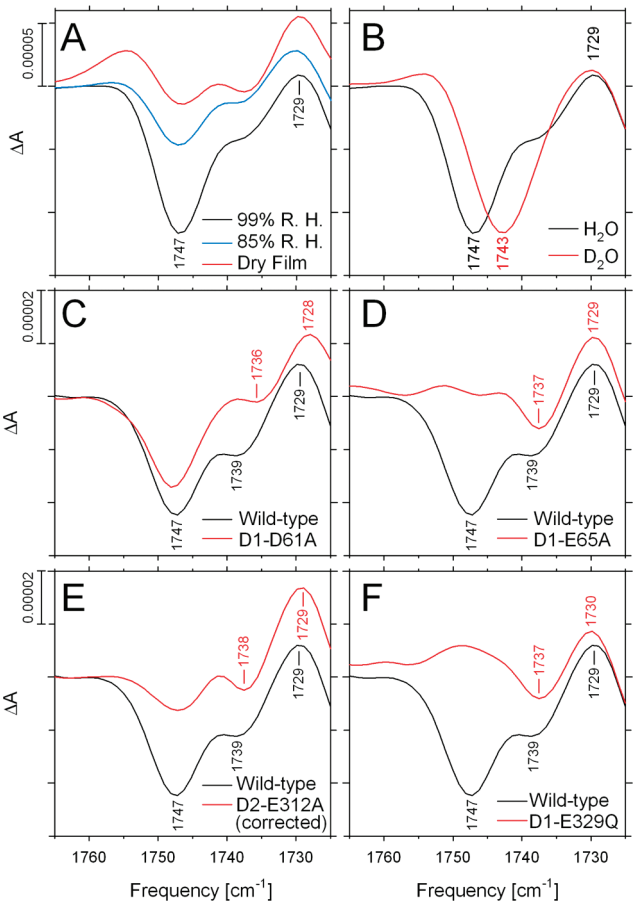

FIGURE 8: ν(C=O) region of the S_2-minus-S_1 FTIR difference spectra of (A) wild-type PSII core complexes maintained at a relative humidity of 99% (black) or 85% (blue) or as a dry film in the sample cell (red), (B) wild-type PSII core complexes exchanged into FTIR buffer containing H_2O (black) or D_2O (red), (C) wild-type (black) and D1-D61A (red) PSII core complexes, (D) wild-type (black) and D1-E65A (red) PSII core complexes, (E) wild-type (black) and D1-E312A (red) PSII core complexes [after correction of D2-E312A for the presence of Mn-depleted reaction centers (see the text for details)], and (F) wild-type (black) and D1-E329Q (red) PSII core complexes. The data have been reproduced from Figures 1A,B, 2, 3, 5, and 6, respectively.

Asp/Glu residues gives rise to positive and negative bands of approximately equal amplitudes [assuming that the two ν(C=O) modes are well separated]. A change in the environment of a carboxylic acid causes the band to shift and gives rise to a differential band. The shape of the negative 1747 cm^{-1} peak in wild-type PSII core complexes suggests that a carboxylate residue partly deprotonates (i.e., its pK_a decreases) in response to the S_1 to S_2 transition. The partial depronation of this residue should increase the amplitudes of the $\nu_{asym}(COO^-)$ and $\nu_{sym}(COO^-)$ modes of the same residue in its carboxylate form. These modes should appear near 1580−1560 and 1400 cm^{-1}, respectively (*72*). Consequently, the loss of the negative peak at 1747 cm^{-1} should correlate with a loss of positive spectral features (or the increase in negative spectral features) near 1580−1560 and 1400 cm^{-1}. Although a decreased positive amplitude at 1587 cm^{-1} is observed in the S_2-minus-S_1 FTIR difference spectrum of partly dehydrated wild-type PSII (blue and red traces in Figure 1A), the same change is not observed in D1-E65A, D2-E312A, or D1-E329Q (top traces in Figures 3, 5, and 6, respectively). Similarly, while an increased negative amplitude near 1400 cm^{-1} is observed in the S_2-minus-S_1 FTIR difference spectra of D1-E65A, D2-E312A, and D1-E329Q (Figures 3, 5, and 6), the same change

is not observed in the partly dehydrated wild type (Figure 1A). We presume that the expected changes to the $\nu_{asym}(COO^-)$ and $\nu_{sym}(COO^-)$ modes are masked by other mutation-induced or dehydration-induced structural changes in these regions.

The structural response of PSII to the development of charge on the Mn_4Ca cluster during the S_1 to S_2 transition presumably is propagated both electrostatically and through networks of hydrogen bonds involving amino acid residues and water molecules. We propose that this propagated structural response alters the environment of the carboxylate group responsible for the 1747 cm^{-1} band, decreasing this group's pK_a value. We also propose that D1-Glu65, D2-Glu312, and D1-Glu329 participate in the same network of hydrogen bonds as the carboxylate group responsible for this band. Finally, we propose that the mutation of any of these three residues to a nonprotonatable residue, or the partial dehydration caused by maintaining samples at a relative humidity of ≤85%, disrupts the network sufficiently that the structural perturbations associated with the S_1 to S_2 transition are no longer transmitted to this carboxylate, thereby eliminating the 1747 cm^{-1} band from the spectrum. The carboxylate group that corresponds to the 1747 cm^{-1} band could be the side chain of D1-Glu65, D2-Glu312, or D1-Glu329. Alternatively, it could belong to another carboxylate residue located in the same proposed network of hydrogen-bonded side chains and water molecules. Because the side chain of D1-Glu329 is located ~20 Å from D1-Glu65 and D2-Glu312 in the 2.9 Å crystallographic structural model (*5*), the extended network of hydrogen bonds identified in this study must extend for at least 20 Å across the lumenal face of the Mn_4Ca cluster and probably includes the chloride ion identified in this model. The existence of extensive networks of hydrogen bonds in the lumenal domains of PSII was predicted recently on the basis of a molecular dynamics study (*36*). Because mutations of D1-Asp61, D1-Glu65, and D2-Glu312 substantially decrease the fraction of PSII reaction centers that undergo the S_3 to S_0 transition in response to a saturating flash, the hydrogen-bonded network that includes these residues may form part of a dominant proton egress pathway leading from the Mn_4Ca cluster to the thylakoid lumen. In is noteworthy that D1-Glu329 does not form part of the same putative access/egress channel as D1-Asp61, D1-Glu65, and D2-Glu312 in recent analyses of static PSII structures (*1*, *5*, *32*−*35*). It is an open question whether features of this network, particularly the apparent connection between D1-Glu329 and the other three residues, exist permanently or fleetingly, like the networks of hydrogen bonds that transiently connect hydrophilic pockets in the recent molecular dynamics study (*36*).

In the 2.9 Å crystallographic structural model, the side chain of D1-Asp61 is located only 4.8 Å from the side chain of D1-Glu65 and only 6.4 Å from the side chain of D2-Glu312 (*5*). Furthermore, D1-Asp61 is located between the Mn_4Ca cluster and both of these residues. Consequently, it seems likely that D1-Asp61 participates in the same network of hydrogen bonds as D1-Glu65, D2-Glu312, and D1-Glu329. Nevertheless, the 1747 cm^{-1} band is unaltered by the mutation of D1-Asp61 to Ala. This lack of an effect provides a constraint on attempts to identify the source of the 1747 cm^{-1} band and suggests that the carboxylate residue that gives rise to this band is located closer to D1-Glu65, D2-Glu312, or D1-Glu329 than to D1-Asp61. Possible candidates include D2-Glu302, D2-Glu308, D2-Glu310, D2-Glu323, PsbO-Asp184, and PsbO-Asp250.

Comparison of the individual FTIR difference spectra of wild-type PSII core particles (e.g., Figure 2, black traces) shows that the negative band at 1747 cm^{-1} in the S_2-minus-S_1 spectrum appears to correlate with a positive band at 1747 cm^{-1} in the S_0-minus-S_3 spectrum and that a positive band at 1745 cm^{-1} in the S_3-minus-S_2 spectrum appears to correlate with a negative band at 1745 cm^{-1} in the S_1-minus-S_0 spectrum. It is tempting to speculate that the structural perturbations responsible for the negative 1747 cm^{-1} band during the S_1 to S_2 transition are reversed during the S_3 to S_0 transition and that another carboxylate group has its pK_a increased during the S_2 to S_3 transition and restored during the S_0 to S_1 transition. It is interesting to note that the 1745 cm^{-1} band was eliminated by all four mutants examined in this study. However, conclusions regarding the reversibility of the 1747 cm^{-1} band and the nature of the 1745 cm^{-1} band must await D_2O exchange analysis of the S_3-minus-S_2, S_0-minus-S_3, and S_1-minus-S_0 transitions in wild-type PSII core complexes.

In PSII core complexes from the cyanobacterium *T. elongatus*, the S_2-minus-S_1 FTIR difference spectrum contains no large negative features at 1747 cm^{-1} (*51*, *66*, *74*−*76*). Furthermore, the exchange of *T. elongatus* PSII core complexes into D_2O produces no downshift of any mode in the ν(C=O) region (*51*). The band is also absent from the S_2-minus-S_1 FTIR difference spectrum of spinach PSII membranes (*77*−*80*), although a positive band at 1747 cm^{-1} was reported in spinach PSII core complexes (*129*). Exchange of spinach PSII membranes into D_2O also produces no downshift of any mode in the ν(C=O) region (*78*). One possible explanation for the lack of this band in *T. elongatus* and spinach PSII preparations derives from the slight differences between the amino acid sequences of the PSII polypeptides of spinach, *T. elongatus*, and *Synechocystis* sp. PCC 6803. Because the sequences differ, the orientations of side chains and water molecules in the extended network of hydrogen bonds are likely to differ. Perhaps these networks differ to the extent that the structural perturbations associated with the S_1 to S_2 transition in *T. elongatus* and spinach are not transmitted to the carboxylate group that is responsible for the 1747 cm^{-1} band in *Synechocystis* sp. PCC 6803. The sensitivity of this band to the extent of sample hydration and to the mutation of selected single amino acid residues shows the sensitivity of the corresponding carboxylate group to minor changes in the protein environment. Alternatively, this carboxylate residue may not be conserved in all organisms. However, a third explanation is that the observation of this band is preparation-dependent. For example, this band has been reported previously in some PSII preparations from *Synechocystis* sp. PCC 6803 (*61*, *62*, *64*, *65*, *69*, *70*), but not in others (*85*, *87*−*89*, *130*). Nevertheless, we have observed it under a variety of conditions, including in PSII core complexes that have been purified in the presence of 25% (v/v) glycerol instead of 1.2 M betaine.

CONCLUDING REMARKS

On the basis of the presence or absence of the ν(C=O) mode of a protonated carboxylate group in the S_2-minus-S_1 FTIR difference spectrum, we conclude that residues D1-Glu65, D1-Glu329, and D2-Glu312 participate in a hydrogen-bonded network that extends at least 20 Å across the lumenal face of the Mn_4Ca cluster. This network presumably also includes D1-Asp61. The D1-D61A, D1-E65A, and D2-E312A mutations appear to substantially decrease the fraction of PSII reaction centers that undergo the S_3 to S_0 transition in response to a saturating flash. Consequently, elements of the hydrogen-bonded network that

includes D1-Asp61, D1-Glu65, D2-Glu312, and D1-Glu329 may comprise part of a dominant proton egress pathway leading from the Mn_4Ca cluster to the thylakoid lumen.

ACKNOWLEDGMENT

We are grateful to Melodie A. Strickler for assistance during the initial phase of this study and to Anh P. Nguyen for maintaining the mutant and wild-type cultures of *Synechocystis* sp. PCC 6803 and for purifying the thylakoid membranes that were used for the isolation of the PSII core complexes. We also thank Athina Zouni and Azat Gabdulkhakov for providing the coordinates for the substrate/product channels included in Figure 7.

REFERENCES

1. Ferreira, K. N., Iverson, T. M., Maghlaoui, K., Barber, J., and Iwata, S. (2004) Architecture of the Photosynthetic Oxygen-Evolving Center. *Science 303*, 1831–1838.
2. Loll, B., Kern, J., Saenger, W., Zouni, A., and Biesiadka, J. (2005) Towards Complete Cofactor Arrangement in the 3.0 Å Resolution Structure of Photosystem II. *Nature 438*, 1040–1044.
3. Kern, J., Biesiadka, J., Loll, B., Saenger, W., and Zouni, A. (2007) Structure of the Mn_4-Ca Cluster as Derived from X-ray Diffraction. *Photosynth. Res. 92*, 389–405.
4. Barber, J. (2008) Crystal Structure of the Oxygen-Evolving Complex of Photosystem II. *Inorg. Chem. 47*, 1700–1710.
5. Guskov, A., Kern, J., Gabdulkhakov, A., Broser, M., Zouni, A., and Saenger, W. (2009) Cyanobacterial Photosystem II at 2.9-Å Resolution and the Role of Quinones, Lipids, Channels, and Chloride. *Nat. Struct. Mol. Biol. 16*, 334–342.
6. Guskov, A., Gabdulkhakov, A., Broser, M., Glöckner, C., Hellmich, J., Kern, J., Frank, J., Müh, F., Saenger, W., and Zouni, A. (2010) Recent Progress in the Crystallographic Studies of Photosystem II. *ChemPhysChem 11*, 1160–1171.
7. McEvoy, J. P., and Brudvig, G. W. (2006) Water-Splitting Chemistry of Photosystem II. *Chem. Rev. 106*, 4455–4483.
8. McCarrick, R. M., and Britt, R. D. (2008) Current Models and Mechanism of Water Splitting. In Photosynthetic Protein Complexes (Fromme, P., Ed.) pp 107−136, Wiley-VCH Verlag GmbH & Co. KGaA, Weinheim, Germany.
9. Rappaport, F., and Diner, B. A. (2008) Primary Photochemistry and Energetics Leading to the Oxidation of the $(Mn)_4Ca$ Cluster and to the Evolution of Molecular Oxygen in Photosystem II. *Coord. Chem. Rev. 252*, 259–272.
10. Renger, G., and Renger, T. (2008) Photosystem II: The Machinery of Photosynthetic Water Splitting. *Photosynth. Res. 98*, 53–80.
11. Yano, J., and Yachandra, V. K. (2008) Where Water is Oxidized to Dioxygen: Structure of the Photosynthetic Mn_4Ca Cluster from X-ray Spectroscopy. *Inorg. Chem. 47*, 1711–1726.
12. Yano, J., and Yachandra, V. K. (2007) Oxidation State Changes of the Mn_4Ca Cluster in Photosystem II. *Photosynth. Res. 92*, 289–303.
13. Dau, H., and Haumann, M. (2008) The Manganese Complex of Photosystem II in its Reaction Cycle: Basic Framework and Possible Realization at the Atomic Level. *Coord. Chem. Rev. 252*, 273–295.
14. Sauer, K., Yano, J., and Yachandra, V. K. (2008) X-ray Spectrsocopy of the Photosynthetic Oxygen-Evolving Complex. *Coord. Chem. Rev. 252*, 318–335.
15. Murray, J. W., Maghlaoui, K., Kargul, J., Ishida, N., Lai, T.-L., Rutherford, A. W., Sugiura, M., Boussac, A., and Barber, J. (2008) X-ray Crystallography Identifies two Chloride Binding Sites in the Oxygen Evolving Centre of Photosystem II. *Energy Environ. Sci. 1*, 161–166.
16. Kawakami, K., Umena, Y., Kamiya, N., and Shen, J.-R. (2009) Location of Chloride and its Possible Functions in Oxygen-Evolving Photosystem II Revealed by X-ray Crystallography. *Proc. Natl. Acad. Sci. U.S.A. 106*, 8567–8572.
17. Yano, J., Kern, J., Irrgang, K.-D., Latimer, M. J., Bergmann, U., Glatzel, P., Pushkar, Y., Biesiadka, J., Loll, B., Sauer, K., Messinger, J., Zouni, A., and Yachandra, V. K. (2005) X-ray Damage to the Mn_4Ca Complex in Single Crystals of Photosystem II: A Case Study for Metalloprotein Crystallography. *Proc. Natl. Acad. Sci. U.S.A. 102*, 12047–12052.
18. Grabolle, M., Haumann, M., Müller, C., Liebisch, P., and Dau, H. (2006) Rapid Loss of Structural Motifs in the Manganese Complex of Oxygenic Photosynthesis by X-ray Irradiation at 10−300 K. *J. Biol. Chem. 281*, 4580–4588.
19. Yano, J., Kern, J., Sauer, K., Latimer, M. J., Pushkar, Y., Biesiadka, J., Loll, B., Saenger, W., Messinger, J., Zouni, A., and Yachandra, V. K. (2006) Where Water is Oxidized to Dioxygen: Structure of the Photosynthetic Mn_4Ca Cluster. *Science 314*, 821–825.
20. Debus, R. J. (2008) Protein Ligation of the Photosynthetic Oxygen-Evolving Center. *Coord. Chem. Rev. 252*, 244–258.
21. Dau, H., and Haumann, M. (2007) Time Resolved X-ray Spectroscopy Leads to an Extension of the Classical S-State Cycle Model of Photosynthetic Oxygen Evolution. *Photosynth. Res. 92*, 327–343.
22. Sproviero, E. M., Gascón, J. A., McEvoy, J. P., Brudvig, G. W., and Batista, V. S. (2008) Computation Studies of the O_2-Evolving Complex of Photosystem II and Biomimetic Oxomanganese Complexes. *Coord. Chem. Rev. 252*, 395–415.
23. Wydrzynski, T., Hillier, W., and Messinger, J. (1996) On the Functional Significance of Substrate Accessibility in the Photosynthetic Water Oxidation Mechanism. *Physiol. Plant. 96*, 342–350.
24. Anderson, J. M. (2001) Does Functional Photosystem II Complex have an Oxygen Channel? *FEBS Lett. 488*, 1–4.
25. McEvoy, J. P., and Brudvig, G. W. (2004) Structure-Based Mechanism of Photosynthetic Water Oxidation. *Phys. Chem. Chem. Phys. 6*, 4754–4763.
26. Haumann, M., Liebisch, P., Müller, C., Barra, M., Grabolle, M., and Dau, H. (2005) Photosynthetic O_2 Formation Tracked by Time-Resolved X-ray Experiments. *Science 310*, 1019–1021.
27. Sproviero, E. M., Gascón, J. A., McEvoy, J. P., Brudvig, G. W., and Batista, V. S. (2008) Quantum Mechanics/Molecular Mechanics Study of the Catalytic Cycle of Water Splitting In Photosystem II. *J. Am. Chem. Soc. 130*, 3428–3442.
28. Sproviero, E. M., McEvoy, J. P., Gascón, J. A., Brudvig, G. W., and Batista, V. S. (2008) Computational Insights into the O_2-Evolving Complex of Photosystem II. *Photosynth. Res. 97*, 91–114.
29. Barber, J., Ferreira, K. N., Maghlaoui, K., and Iwata, S. (2004) Structural Model of the Oxygen-Evolving Centre of Photosystem II with Mechanistic Implications. *Phys. Chem. Chem. Phys. 6*, 4737–4742.
30. De Las Rivas, J., and Barber, J. (2004) Analysis of the Structure of the PsbO Protein and Its Implications. *Photosynth. Res. 81*, 329–343.
31. Shutova, T., Klimov, V. V., Andersson, B., and Samuelsson, G. (2007) A Cluster of Carboxylic Groups in PsbO Protein is Involved in Proton Transfer from the Water Oxidizing Complex of Photosystem II. *Biochim. Biophys. Acta 1767*, 434–440.
32. Ishikita, H., Saenger, W., Loll, B., Biesiadka, J., and Knapp, E.-W. (2006) Energetics of a Possible Proton Exit Pathway for Water Oxidation in Photosystem II. *Biochemistry 45*, 2063–2071.
33. Ho, F. M., and Styring, S. (2008) Access Channels and Methanol Binding Site to the $CaMn_4$ Cluster in Photosystem II based on Solvent Accessibility Simulation, with Implications for Substrate Water Access. *Biochim. Biophys. Acta 1777*, 140–153.
34. Murray, J. W., and Barber, J. (2007) Structural Characteristics of Channels and Pathways in Photosystem II Including the Identification of an Oxygen Channel. *J. Struct. Biol. 159*, 228–237.
35. Gabdulkhakov, A., Guskov, A., Broser, M., Kern, J., Müh, F., Saenger, W., and Zouni, A. (2009) Probing the Accessibility of the Mn_4Ca Cluster in Photosystem II: Channels Calculation, Noble Gas Derivatization, and Cocrystallization with DMSO. *Structure 17*, 1223–1234.
36. Vassiliev, S., Comte, P., Mahboob, A., and Bruce, D. (2010) Tracking the Flow of Water through Photosystem II Using Molecular Dynamics and Streamline Tracing. *Biochemistry 49*, 1873–1881.
37. Okamura, M. Y., Paddock, M. L., Graige, M. S., and Feher, G. (2000) Proton and electron transfer in bacterial reaction centers. *Biochim. Biophys. Acta 1458*, 148–163.
38. Paddock, M. L., Feher, G., and Okamura, M. Y. (2003) Proton Transfer Pathways and Mechanism in Bacterial Reaction Centers. *FEBS Lett. 555*, 45–50.
39. Wraight, C. A. (2005) Intraprotein Proton Transfer: Concepts and Realities from the Bacterial Photosynthetic Reaction Center. In Biophysical and Structural Aspects of Bioenergetics (Wikström, M., Ed.) pp 273−313, Royal Society of Chemistry, Cambridge, U.K.
40. Zscherp, C., and Barth, A. (2001) Reaction-Induced Infrared Difference Spectroscopy for the Study of Protein Reaction Mechanisms. *Biochemistry 40*, 1875–1883.
41. Barth, A., and Zscherp, C. (2002) What Vibrations Tell Us About Proteins. *Q. Rev. Biophys. 35*, 369–430.
42. Rich, P. R., and Iwaki, M. (2005) Infrared Protein Spectroscopy as a Tool to Study Protonation Reactions Within Proteins. In Biopysical and Structural Aspects of Bioenergetics (Wikström, M., Ed.) pp 314−333, Royal Society of Chemistry, Cambridge, U.K.

43. Barth, A. (2007) Infrared Spectroscopy of Proteins. *Biochim. Biophys. Acta 1767*, 1073–1101.
44. Berthomieu, C., and Hienerwadel, R. (2009) Fourier Transform Infrared (FTIR) Spectroscopy. *Photosynth. Res. 101*, 157–170.
45. Maeda, A., Sasaki, J., Shichida, Y., Yoshizawa, Y., Chang, M., Ni, B., Needleman, R., and Lanyi, J. K. (1992) Structures of Aspartic Acid-96 in the L and N Intermediates of Bacteriorhodopsin: Analysis by Fourier Transform Infrared Spectroscopy. *Biochemistry 31*, 4684–4690.
46. Dioumaev, A. K., and Braiman, M. S. (1995) Modeling Vibrational Spectra of Amino Acid Side Chains in Proteins: The Carbonyl Stretch Frequency of Buried Carboxylic Side Chains. *J. Am. Chem. Soc. 117*, 10572–10574.
47. Dioumaev, A. K. (2001) Infrared Methods for Monitoring the Protonation State of Carboxylic Amino Acids in the Photocycle of Bacteriorhodopsin. *Biochemistry* (*Moscow, Russ. Fed.*) *66*, 1269–1276.
48. Nie, B., Stutzman, J., and Xie, A. (2005) A Vibrational Spectral Marker for Probing the Hydrogen-Bonding Status of Protonated Asp and Glu Residues. *Biophys. J. 88*, 2833–2847.
49. Takei, K.-I., Takahashi, R., and Noguchi, T. (2008) Correlation Between the Hydrogen-Bond Structures and the C=O Stretching Frequencies of Carboxylic Acids as Studied by Density Functional Theory Calculations: Theoretical Basis for Interpretation of Infrared Bands of Carboxylic Groups in Proteins. *J. Phys. Chem. B 112*, 6725–6731.
50. Noguchi, T., and Sugiura, M. (2000) Structure of an Active Water Molecule in the Water-Oxidizing Complex of Photosystem II as Studied by FTIR Spectroscopy. *Biochemistry 39*, 10943–10949.
51. Noguchi, T., and Sugiura, M. (2002) FTIR Detection of Water Reactions During the Flash-Induced S-State Cycle of the Photosynthetic Water-Oxidizing Complex. *Biochemistry 41*, 15706–15712.
52. Noguchi, T. (2007) FTIR Detection of Water Reactions in the Oxygen-Evolving Center of Photosystem II. *Philos. Trans. R. Soc. London, Ser. B 363*, 1189–1195.
53. Venyaminov, S. Yu., and Prendergast, F. G. (1997) Water (H_2O and D_2O) Molar Aborptivity in the 1000−4000 cm^{-1} Range and Quantitative Infrared Spectroscpy of Aqueous Solutions. *Anal. Biochem. 248*, 234–245.
54. Suzuki, H., Sugiura, M., and Noguchi, T. (2008) Monitoring Water Reactions during the S-State Cycle of the Photosynthetic Water-Oxidizing Center: Detection of the DOD Bending Vibrations by Means of Fourier Transform Infrared Spectroscopy. *Biochemistry 47*, 11024–11030.
55. Noguchi, T., and Berthomieu, C. (2005) Molecular Analysis by Vibrational Spectroscopy. In Photosystem II: The Light-Driven Water:Plastoquinone Oxidoreductase (Wydrzynski, T., and Satoh, K., Eds.) pp 367−387, Springer, Dordrecht, The Netherlands.
56. Noguchi, T. (2007) Light-Induced FTIR Difference Spectroscopy as a Powerful Tool Toward Understanding the Molecular Mechanism of Photosynthetic Oxygen Evolution. *Photosynth. Res. 91*, 59–69.
57. Noguchi, T. (2008) Fourier Transform Infrared Analysis of the Photosynthetic Oxygen-Evolving Center. *Coord. Chem. Rev. 251*, 336–346.
58. Chu, H.-A., Nguyen, A. P., and Debus, R. J. (1994) Site-Directed Photosystem II Mutants with Perturbed Oxygen Evolving Properties: 1. Instability or Inefficient Assembly of the Manganese Cluster *In Vivo*. *Biochemistry 33*, 6137–6149.
59. Debus, R. J., Campbell, K. A., Gregor, W., Li, Z.-L., Burnap, R. L., and Britt, R. D. (2001) Does Histidine 332 of the D1 Polypeptide Ligate the Manganese Cluster in Photosystem II? An Electron Spin Echo Envelope Modulation Study. *Biochemistry 40*, 3690–3699.
60. Faller, P., Rutherford, A. W., and Debus, R. J. (2002) Tyrosine D Oxidation at Cryogenic Temperature in Photosystem II. *Biochemistry 41*, 12914–12920.
61. Strickler, M. A., Walker, L. M., Hillier, W., Britt, R. D., and Debus, R. J. (2007) No Evidence from FTIR Difference Spectroscopy That Aspartate-342 of the D1 Polypeptide Ligates a Mn Ion That Undergoes Oxidation during the S_0 to S_1, S_1 to S_2, or S_2 to S_3 Transitions in Photosystem II. *Biochemistry 46*, 3151–3160.
62. Strickler, M. A., Walker, L. M., Hillier, W., and Debus, R. J. (2005) Evidence from Biosynthetically Incorporated Strontium and FTIR Difference Spectroscopy that the C-Terminus of the D1 Polypeptide of Photosystem II Does Not Ligate Calcium. *Biochemistry 44*, 8571–8577.
63. Yamanari, T., Kimura, Y., Mizusawa, N., Ishii, A., and Ono, T.-A. (2004) Mid- to Low-Frequency Fourier Transform Infrared Spectra of S-State Cycle for Photosynthetic Water Oxidation in *Synechocystis* sp. PCC 6803. *Biochemistry 43*, 7479–7490.
64. Debus, R. J., Strickler, M. A., Walker, L. M., and Hillier, W. (2005) No Evidence from FTIR Difference Spectroscopy That Aspartate-170 of the D1 Polypeptide Ligates a Manganese Ion That Undergoes Oxidation during the S_0 to S_1, S_1 to S_2, or S_2 to S_3 Transitions in Photosystem II. *Biochemistry 44*, 1367–1374.
65. Strickler, M. A., Hillier, W., and Debus, R. J. (2006) No Evidence from FTIR Difference Spectroscopy that Glutamate-189 of the D1 Polypeptide Ligates a Mn Ion that Undergoes Oxidation During the S_0 to S_1, S_1 to S_2, or S_2 to S_3 Transitions in Photosystem II. *Biochemistry 45*, 8801–8811.
66. Noguchi, T., and Sugiura, M. (2002) Flash-Induced FTIR Difference Spectra of the Water Oxidizing Complex in Moderately Hydrated Photosystem II Core Films: Effect of Hydration Extent on S-State Transitions. *Biochemistry 41*, 2322–2330.
67. Glasoe, P. K., and Long, F. A. (1960) Use of Glass Electrodes to Measure Acidities in Deuterium Oxide. *J. Phys. Chem. 64*, 188–191.
68. Salomaa, P., Schaleger, L. L., and Long, F. A. (1964) Solvent Deuterium Isotope Effects on Acid-Base Equilibria. *J. Am. Chem. Soc. 86*, 1–7.
69. Chu, H.-A., Hillier, W., and Debus, R. J. (2004) Evidence that the C-Terminus of the D1 Polypeptide is Ligated to the Manganese Ion that Undergoes Oxidation During the S_1 to S_2 Transition: An Isotope-Edited FTIR Study. *Biochemistry 43*, 3152–3166.
70. Noguchi, T., Inoue, Y., and Tang, X. S. (1997) Structural coupling between the oxygen-evolving Mn cluster and a tyrosine residue in photosystem II as revealed by Fourier transform infrared spectroscopy. *Biochemistry 36*, 14705–14711.
71. Strickler, M. A., Hwang, H. J., Burnap, R. L., Yano, J., Walker, L. M., Service, R. J., Britt, R. D., Hillier, W., and Debus, R. J. (2008) Glutamate-354 of the CP43 Polypeptide Interacts with the Oxygen-Evolving Mn_4Ca Cluster of Photosystem II: A Preliminary Characterization of the Glu354Gln Mutant. *Philos. Trans. R. Soc. London, Ser. B 363*, 1179–1188.
72. Barth, A. (2000) The Infrared Absorption of Amino Acid Side Chains. *Prog. Biophys. Mol. Biol. 74*, 141–173.
73. Socrates, G. (2001) Infrared Characteristic Group Frequencies: Tables and Charts, 3rd ed., John Wiley & Sons, Chichester, U.K.
74. Noguchi, T., and Sugiura, M. (2003) Analysis of Flash-Induced FTIR Difference Spectra of the S-State Cycle in the Photosynthetic Water-Oxidizing Complex by Uniform ^{15}N and ^{13}C Isotope Labeling. *Biochemistry 42*, 6035–6042.
75. Suzuki, H., Sugiura, M., and Noguchi, T. (2005) pH Dependence of the Flash-Induced S-State Transitions in the Oxygen-Evolving Center of Photosystem II from *Thermosynechococcus elongatus* as Revealed by Fourier Transform Infrared Spectroscopy. *Biochemistry 44*, 1708–1718.
76. Suzuki, H., Sugiura, M., and Noguchi, T. (2009) Monitoring Proton Release during Photosynthetic Water Oxidation in Photosystem II by Means of Isotope-Edited Infrared Spectroscopy. *J. Am. Chem. Soc. 131*, 7849–7857.
77. Noguchi, T., Ono, T.-A., and Inoue, Y. (1995) Direct Detection of a Carboxylate Bridge Between Mn and Ca^{2+} in the Photosynthetic Oxygen-Evolving Center by Means of Fourier Transform Infrared Spectroscopy. *Biochim. Biophys. Acta 1228*, 189–200.
78. Noguchi, T., Ono, T.-A., and Inoue, Y. (1995) A Carboxylate Ligand Interacting with Water in the Oxygen-Evolving Center of Photosystem II as Revealed by Fourier Transform Infrared Spectroscopy. *Biochim. Biophys. Acta 1232*, 59–66.
79. Onoda, K., Mino, H., Inoue, Y., and Noguchi, T. (2000) An FTIR study on the structure of the oxygen-evolving Mn-cluster of Photosystem II in different spin forms of the S_2 state. *Photosynth. Res. 63*, 47–57.
80. Kimura, Y., Hasegawa, K., Yamanari, T., and Ono, T.-A. (2005) Studies on Photosynthetic Oxygen-Evolving Complex by Means of Fourier Transform Infrared Spectroscopy: Calcium and Chloride Cofactors. *Photosynth. Res. 84*, 245–250.
81. Noguchi, T., Sugiura, M., and Inoue, Y. (1999) FTIR Studies on the Amino-Acid Ligands of the Photosynthetic Oxygen-Evolving Mn-Cluster. In Fourier Transform Spectroscopy: Twelfth International Conference (Itoh, K., and Tasumi, M., Eds.) pp 459−460, Waseda University Press, Tokyo.
82. Kimura, Y., Mizusawa, N., Ishii, A., Yamanari, T., and Ono, T.-A. (2003) Changes of Low-Frequency Vibrational Modes Induced by Universal ^{15}N- and ^{13}C-Isotope Labeling in S2/S1 FTIR Difference Spectrum of Oxygen-Evolving Complex. *Biochemistry 42*, 13170–13177.
83. Chu, H.-A., Nguyen, A. P., and Debus, R. J. (1995) Amino Acid Residues that Influence the Binding of Manganese or Calcium to Photosystem II. 2. The Carboxy-terminal Domain of the D1 Polypeptide. *Biochemistry 34*, 5859–5882.

84. Chu, H.-A., Nguyen, A. P., and Debus, R. J. (1995) Amino Acid Residues that Influence the Binding of Manganese or Calcium to Photosystem II. 1. The Lumenal Inter-Helical Domains of the D1 Polypeptide. *Biochemistry 34*, 5839–5858.
85. Shimada, Y., Suzuki, H., Tsuchiya, T., Tomo, T., Noguchi, T., and Mimuro, M. (2009) Effect of a Single-Amino Acid Substitution of the 43 kDa Chlorophyll Protein on the Oxygen-Evolving Reaction of the Cyanobacterium *Synechocystis* sp. PCC 6803: Analysis of the Glu354Gln Mutation. *Biochemistry 48*, 6095–6103.
86. Berthomieu, C., Hienerwadel, R., Boussac, A., Breton, J., and Diner, B. A. (1998) Hydrogen-Bonding of Redox-Active Tyrosine Z of Photosystem II Probed by FTIR Difference Spectroscopy. *Biochemistry 37*, 10547–10554.
87. Chu, H.-A., Debus, R. J., and Babcock, G. T. (2001) D1-Asp170 is Structurally Coupled to the Oxygen Evolving Complex in Photosystem II as Revealed by Light-Induced Fourier Transform Infrared Difference Spectroscopy. *Biochemistry 40*, 2312–2316.
88. Kimura, Y., Mizusawa, N., Ishii, A., Nakazawa, S., and Ono, T.-A. (2005) Changes in Structural and Functional Properties of Oxygen-Evolving Complex Induced by Replacement of D1-Glutamate 189 with Glutamine in Photosystem II: Ligation of Glutamate 189 Carboxylate to the Manganese Cluster. *J. Biol. Chem. 280*, 37895–37900.
89. Kimura, Y., Mizusawa, N., Yamanari, T., Ishii, A., and Ono, T.-A. (2005) Structural Changes of D1 C-terminal α-Carboxylate during S-state Cycling of Photosynthetic Oxygen Evolution. *J. Biol. Chem. 280*, 2078–2083.
90. Londergan, C. H., and Kubiak, C. P. (2003) Electron Transfer and Dynamic Infrared-Band Coalescence: It looks like Dynamic NMR Spectroscopy, but a Billion Times Faster. *Chem.—Eur. J. 9*, 5962–5969.
91. Glover, S. D., Goeltz, J. C., Lear, B. J., and Kubiak, C. P. (2009) Mixed Valency at the Nearly Delocalized Limit: Fundamentals and Forecast. *Eur. J. Inorg. Chem. 2009*, 585–594.
92. Goeltz, J. C., Hanson, C. J., and Kubiak, C. P. (2009) Rates of Electron Self-Exchange Reactions between Oxo-Centered Ruthenium Clusters are Determined by Orbital Overlap. *Inorg. Chem. 48*, 4763–4767.
93. Glatzel, P., Bergmann, U., Yano, J., Visser, H., Robblee, J. H., Gu, W., De Groot, F. M. F., Christou, G., Pecoraro, V. L., Cramer, S. P., and Yachandra, V. K. (2004) The Electronic Structure of Mn in Oxides, Coordination Complexes, and the Oxygen-Evolving Complex of Photosystem II Studied by Resonant Inelastic X-ray Scattering. *J. Am. Chem. Soc. 126*, 9946–9959.
94. Sproviero, E. M., Gascón, J. A., McEvoy, J. P., Brudvig, G. W., and Batista, V. S. (2006) QM/MM Models of the O_2-Evolving Complex of Photosystem II. *J. Chem. Theory Comput. 2*, 1119–1134.
95. Stull, J. A., Stich, T. A., Service, R. J., Debus, R. J., Mandal, S. K., Armstrong, W. H., and Britt, R. D. (2010) ^{13}C ENDOR Reveals that the D1 Polypeptide C-Terminus is Directly Bound to Mn in the Photosystem II Oxygen Evolving Complex. *J. Am. Chem. Soc. 132*, 446–447.
96. Iizasa, M., Suzuki, H., and Noguchi, T. (2010) Orientations of Carboxylate Groups Coupled to the Mn Cluster in the Photosynthetic Oxygen-Evolving Center as Studied by Polarized ATR-FTIR Spectroscopy. *Biochemistry 49*, 3074–3082.
97. Cohen, R. O., Nixon, P. J., and Diner, B. A. (2007) Participation of the C-terminal Region of the D1-Polypeptide in the First Steps in the Assembly of the Mn_4Ca Cluser of Photosystem II. *J. Biol. Chem. 282*, 7209–7218.
98. Hwang, H. J., McLain, A., Debus, R. J., and Burnap, R. L. (2007) Photoassembly of the Manganese Cluster in Mutants Perturbed in the High Affinity Mn-Binding Site of the H_2O-Oxidation Complex of Photosystem II. *Biochemistry 46*, 13648–13657.
99. Debus, R. J. (2001) Amino Acid Residues that Modulate the Properties of Tyrosine Y_Z and the Manganese Cluster in the Water Oxidizing Complex of Photosystem II. *Biochim. Biophys. Acta 1503*, 164–186.
100. Diner, B. A. (2001) Amino Acid Residues Involved in the Coordination and Assembly of the Manganese Cluster of Photosystem II. Proton-Coupled Electron Transport of the Redox-Active Tyrosines and Its Relationship to Water Oxidation. *Biochim. Biophys. Acta 1503*, 147–163.
101. Debus, R. J. (2005) The Catalytic Manganese Cluster: Protein Ligation. In Photosystem II: The Light-Driven Water:Plastoquinone Oxidoreductase (Wydrzynski, T., and Satoh, K., Eds.) pp 261−284, Springer, Dordrecht, The Netherlands.
102. Tommos, C., and Babcock, G. T. (2000) Proton and Hydrogen Currents in Photosynthetic Water Oxidation. *Biochim. Biophys. Acta 1458*, 199–219.
103. Wraight, C. A. (2006) Chance and Design: Proton Transfer in Water, Channels and Bioenergetic Proteins. *Biochim. Biophys. Acta 1757*, 886–912.
104. Silverman, D. N., and McKenna, R. (2007) Solvent-Mediated Proton Transfer in Catalysis by Carbonic Anhydrase. *Acc. Chem. Res. 40*, 669–675.
105. Mikulski, R. L., and Silverman, D. N. (2010) Proton Transfer in Catalysis and the Role of Proton Shuttles in Carbonic Anhydrase. *Biochim. Biophys. Acta 1804*, 422–426.
106. Hosler, J. P., Ferguson-Miller, S., and Mills, D. A. (2006) Energy Transduction: Proton Transfer Through the Respiratory Complexes. *Annu. Rev. Biochem. 75*, 165–187.
107. Wikström, M., and Verkhovsky, M. I. (2007) Mechanism and Energetics of Proton Translocation by the Respiratory Heme-Copper Oxidases. *Biochim. Biophys. Acta 1767*, 1200–1214.
108. Brzezinski, P., and Gennis, R. B. (2008) Cytochrome c Oxidase: Exciting Progress and Remaining Mysteries. *J. Bioenerg. Biomembr. 40*, 521–531.
109. Hundelt, M., Hays, A.-M. A., Debus, R. J., and Junge, W. (1998) Oxygenic Photosystem II: The Mutation D1-D61N in *Synechocystis* sp. PCC 6803 Retards S-State Transitions without Affecting Electron Transfer from Y_Z to P_{680}^+. *Biochemistry 37*, 14450–14456.
110. Hundelt, M., Hays, A.-M. A., Debus, R. J., and Junge, W. (1998) The Mutation D1-D61N in PSII of *Synechocystis*: Retardation of ET from OEC→Y_Z^{ox} and No Effect on Y_Z→P_{680}^+. In Photosynthesis: Mechanisms and Effects (Garab, G., Ed.) Vol. *II*, pp 1387−1390, Kluwer Academic Publishers, Dordrecht, The Netherlands.
111. Qian, M., Dao, L., Debus, R. J., and Burnap, R. L. (1999) Impact of Mutations within the Putative Ca^{2+}-Binding Lumenal Interhelical a-b Loop of the Photosystem II D1 Protein on the Kinetics of Photoactivation and H_2O-Oxidation in *Synechocystis* sp. PCC 6803. *Biochemistry 38*, 6070–6081.
112. Ananyev, G., Nguyen, T., Putnam-Evans, C., and Dismukes, G. C. (2005) Mutagenesis of CP43-Arginine-357 to Serine Reveals New Evidence for (Bi)Carbonate Functioning in the Water Oxidizing Complex of Photosystem II. *Photochem. Photobiol. Sci. 4*, 991–998.
113. Hwang, H. J., Dilbeck, P., Debus, R. J., and Burnap, R. L. (2007) Mutation of Arginine 357 of the CP43 Protein of Photosystem II Severely Impairs the Catalytic S-State Cycle of the H_2O Oxidation Complex. *Biochemistry 46*, 11987–11997.
114. Siebert, F., Mäntele, W., and Kreutz, W. (1982) Evidence for the Protonation of Two Internal Carboxylic Groups During the Photocycle of Bacteriorhodopsin. *FEBS Lett. 141*, 82–87.
115. Engelhard, M., Gerwert, K., Hess, B., Kreutz, W., and Siebert, F. (1985) Light-Driven Protonation Changes of Internal Aspartic Acids of Bacteriorhodopsin: An Investigation by Static and Time-Resolved Infrared Difference Spectroscopy Using [4-^{13}C]Aspartic Acid Labeled Purple Membrane. *Biochemistry 24*, 400–407.
116. Dioumaev, A. K., Richter, H. T., Brown, L. S., Tanio, M., Tuzi, S., Saito, H., Kimura, Y., Needleman, R., and Lanyi, J. K. (1998) Existence of a proton transfer chain in bacteriorhodopsin: Participation of Glu-194 in the release of protons to the extracellular surface. *Biochemistry 37*, 2496–2506.
117. Dioumaev, A. K., Brown, L. S., Needleman, R., and Lanyi, J. K. (1999) Fourier-Transform Infrared Spectra of a Late Intermediate of the Bacteriorhodopsin Photocycle Suggest Transient Protonation of Asp-212. *Biochemistry 38*, 10070–10078.
118. de Grip, W. J., Gillespie, J., and Rothschild, K. J. (1985) Carboxyl Group Involvement in the Meta I and Meta II Stages in Rhodopsin Bleaching: A Fourier Transform Infrared Spectroscopic Study. *Biochim. Biophys. Acta 809*, 97–106.
119. Ganter, U. M., Gärtner, W., and Siebert, F. (1988) Rhodopsin-Lumirhodopsin Phototransition of Bovine Rhodopsin Investigated by Fourier Transform Infrared Difference Spectroscopy. *Biochemistry 27*, 7480–7488.
120. Nabedryk, E., Breton, J., Hienerwadel, R., Fogel, C., Mäntele, W., Paddock, M. L., and Okamura, M. Y. (1995) Fourier Transform Infrared Difference Spectroscopy of Secondary Quinone Acceptor Photoreduction in Proton Transfer Mutants of *Rhodobacter sphaeroides*. *Biochemistry 34*, 14722–14732.
121. Hienerwadel, R., Grzybek, S., Fogel, C., Kreutz, W., Okamura, M. Y., Paddock, M. L., Breton, J., Nabedryk, E., and Mäntele, W. (1995) Protonation of Glu L212 Following Q_B^- Formation in the Photosynthetic Reaction Center of *Rhodobacter sphaeroides*: Evidence from Time-Resolved Infrared Spectroscopy. *Biochemistry 34*, 2832–2843.
122. Nabedryk, E., Breton, J., Okamura, M. Y., and Paddock, M. L. (1998) Proton Uptake by Carboxylic Acid Groups upon Photoreduction of the Secondary Quinone (Q_B) in Bacterial Reaction

Centers from *Rhodobacter sphaeroides*: FTIR Studies on the Effects of Replacing Glu H173. *Biochemistry 37*, 14457–14462.
123. Nabedryk, E., Breton, J., Okamura, M. Y., and Paddock, M. L. (1998) Direct Evidence of Structural Changes in Reaction Centers of *Rb. sphaeroides* Containing Suppressor Mutations for AspL213→Asn: A FTIR Study of Q_B Photoreduction. *Photosynth. Res. 55*, 293–299.
124. Hellwig, P., Rost, B., Kaiser, U., Ostermeier, C., Michel, H., and Mäntele, W. (1996) Carboxyl Group Protonation upon Reduction of the *Paracoccus denitrificans* Cytochrome *c* Oxidase: Direct Evidence by FTIR Spectroscopy. *FEBS Lett. 385*, 53–57.
125. Lübben, M., and Gerwert, K. (1996) Redox FTIR Difference Spectroscopy Using Caged Electrons Reveals Contributions of Carboxyl Groups to the Catalytic Mechanism of Haem-Copper Oxidases. *FEBS Lett. 397*, 303–307.
126. Hellwig, P., Behr, J., Ostermeier, C., Richter, O. M., Pfitzner, U., Odenwald, A., Ludwig, B., Michel, H., and Mäntele, W. (1998) Involvement of Glutamic Acid 278 in the Redox Reaction of the Cytochrome *c* Oxidase from *Paracoccus denitrificans* Investigated by FTIR Spectroscopy. *Biochemistry 37*, 7390–7399.
127. Lübben, M., Prutsch, A., Mamat, B., and Gerwert, K. (1999) Electron Transfer Induces Side-Chain Conformational Changes of Gluamate-286 from Cytochrome bo_3. *Biochemistry 38*, 2048–2056.
128. Xie, A., Hoff, W. D., Kroon, A. R., and Hellingwerf, K. J. (1996) Glu46 Donates a Proton to the 4-Hydroxycinnamate Anion Chromophore During the Photocycle of Photoactive Yellow Protein. *Biochemistry 35*, 14671–14678.
129. Hillier, W., and Babcock, G. T. (2001) S-State Dependent FTIR Difference Spectra for the Photosystem II Oxygen Evolving Complex. *Biochemistry 40*, 1503–1509.
130. Mizusawa, N., Kimura, Y., Ishii, A., Yamanari, T., Nakazawa, S., Teramoto, H., and Ono, T.-A. (2004) Impact of Replacement of D1 C-terminal Alanine with Glycine on Structure and Function of Photosynthetic Oxygen-Evolving Complex. *J. Biol. Chem. 279*, 29622–29627.